

## RESEARCH ARTICLE

# Inhibitory SMAD6 interferes with BMP-dependent generation of muscle progenitor cells and perturbs proximodistal pattern of murine limb muscles

Hasan Asfour<sup>1</sup>, Estelle Hirsinger<sup>2</sup>, Raquel Rouco<sup>3</sup>, Faouzi Zarrouki<sup>1</sup>, Shinichiro Hayashi<sup>4</sup>, Sandra Swist<sup>5</sup>, Thomas Braun<sup>5</sup>, Ketan Patel<sup>6</sup>, Frédéric Relaix<sup>7</sup>, Guillaume Andrey<sup>3</sup>, Sigmar Stricker<sup>8</sup>, Delphine Duprez<sup>2</sup>, Amalia Stantzou<sup>1,\*</sup> and Helge Amthor<sup>1,9,\*</sup>


## ABSTRACT

The mechanism of pattern formation during limb muscle development remains poorly understood. The canonical view holds that naïve limb muscle progenitor cells (MPCs) invade a pre-established pattern of muscle connective tissue, thereby forming individual muscles. Here, we show that early murine embryonic limb MPCs highly accumulate pSMAD1/5/9, demonstrating active signaling of bone morphogenetic proteins (BMP) in these cells. Overexpression of inhibitory human *SMAD6* (*huSMAD6*) in limb MPCs abrogated BMP signaling, impaired their migration and proliferation, and accelerated myogenic lineage progression. Fewer primary myofibers developed, causing an aberrant proximodistal muscle pattern. Patterning was not disturbed when *huSMAD6* was overexpressed in differentiated muscle, implying that the proximodistal muscle pattern depends on BMP-mediated expansion of MPCs before their differentiation. We show that limb MPCs differentially express Hox genes, and Hox-expressing MPCs displayed active BMP signaling. *huSMAD6* overexpression caused loss of HOXA11 in early limb MPCs. In conclusion, our data show that BMP signaling controls expansion of embryonic limb MPCs as a prerequisite for establishing the proximodistal muscle pattern, a process that involves expression of Hox genes.

**KEY WORDS:** PAX3, SMAD6, BMP signaling, Hox, Myogenic progenitor cell, Myogenesis, Muscle fiber, Embryonic muscle, Fetal muscle, Limb muscle, Patterning, Mouse

<sup>1</sup>Université Paris-Saclay, UVSQ, Inserm, END-ICAP, 78000 Versailles, France. <sup>2</sup>Sorbonne Université, Institut Biologie Paris Seine, CNRS UMR7622, Developmental Biology Laboratory, Inserm U1156, 75005 Paris, France. <sup>3</sup>Faculty of Medicine, Department of Genetic Medicine and Development, University of Geneva, 1211 Geneva 4, Switzerland. <sup>4</sup>Department of Neuromuscular Research, National Center of Neurology and Psychiatry (NCNP), National Institute of Neuroscience, Tokyo 187-8502, Japan. <sup>5</sup>Department of Cardiac Development and Remodeling, Max-Planck-Institute for Heart and Lung Research, 61231 Bad Nauheim, Germany. <sup>6</sup>School of Biological Sciences, University of Reading, Reading RG6 6AH, UK. <sup>7</sup>Université Paris Est Créteil, INSERM, EnvA, EFS, AP-HP, IMRB, 94010 Créteil, France. <sup>8</sup>Institute for Chemistry and Biochemistry, Freie Universität Berlin, 14195 Berlin, Germany. <sup>9</sup>Service de Pédiatrie, AP-HP, Hôpital Raymond Poincaré, 92380 Garches, France.

\*Authors for correspondence (helge.amthor@uvsq.fr; amalia.stantzou@uvsq.fr)

 H.Asfour, 0000-0002-4107-3981; E.H., 0000-0002-5256-7741; R.R., 0000-0002-0657-0704; F.Z., 0000-0003-0905-9036; S.H., 0000-0001-5553-7698; S.S., 0000-0002-1269-2177; T.B., 0000-0002-6165-4804; K.P., 0000-0002-7131-749X; F.R., 0000-0003-1270-1472; G.A., 0000-0002-0911-4907; S.S., 0000-0002-7174-5363; D.D., 0000-0003-0248-7417; A.S., 0000-0002-4903-6384; H.Amthor, 0000-0003-1008-719X

Handling Editor: Liz Robertson

Received 6 December 2022; Accepted 2 May 2023

## INTRODUCTION

As in all tetrapods, mammalian limb musculature is derived from a small number of myogenic progenitor cells (MPCs) that migrate from somites into the developing limb bud, where they expand in number, differentiate and form a multitude of individual muscles (Christ and Brand-Saberi, 2002). Migrating limb MPCs are thought to have no positional information but rather rely on signals from their new environment (Blagden and Hughes, 1999). The cues for muscle patterning reside in the limb mesenchymal cells and are independent of the presence of limb MPCs (Grim and Wachtler, 1991; Vallecillo-García et al., 2017). Increasing evidence suggests that individual muscles are formed when MPCs invade a prepattern that is established by muscle connective tissue (MCT) and controlled by a combination of transcription factors, e.g. Hox (Zakany and Duboule, 2007; Swinehart et al., 2013), TBX3 (Colasanto et al., 2016), TBX4/5 (Hasson et al., 2010), TCF4 (Kardon et al., 2003) and OSR1 (Vallecillo-García et al., 2017). However, the connective tissue of limbs without muscle does not form morphologically distinguishable structures that resemble the pattern of individualized muscles – the muscle-devoid space is instead filled with loosely organized mesenchyme and eventually with fat (Christ et al., 1977). Initial tendon formation also occurs independently of muscle; however, the tendons degenerate secondarily if they do not connect to a muscle (Huang et al., 2015).

Opposing the view of ‘myogenic naivety’, the expression of HOXA11 and HOXA13 proteins has been observed in chicken limb MPCs, suggesting that MPCs acquire positional identity. Interestingly, the spatiotemporal dynamics of Hox expression in chicken MPCs are influenced by cues emanating from the apical ectodermal ridge and the zone of polarizing activity. In addition, ectopic application of factors such as fibroblast growth factors (FGFs) and bone morphogenetic proteins (BMPs) were shown to regulate Hox expression in chicken MPCs. These findings suggest that MPCs may follow similar cues during patterning as the limb mesenchyme (Yamamoto et al., 1998; Hashimoto et al., 1999; Yamamoto and Kuroiwa, 2003).

In mice, muscle patterning starts at embryonic day (E)11.5, with successive splitting of premuscle masses into distinct blocks. Individual muscles become distinguishable from E12.5 onwards, and muscle individualization is complete by E14.5 at the end of embryonic myogenesis (Huang, 2017). Although non-muscle cells drive the limb muscle pattern (Kardon et al., 2002; Tozer et al., 2007), MPCs first need to integrate spatiotemporal information for their appropriate positioning, proliferation and differentiation. The molecular mechanisms driving MPC proliferation and differentiation at the right place and time are not fully understood.

BMPs are involved in embryonic MPC expansion in chicken limbs (Amthor et al., 1998; Wang et al., 2010). Moreover, BMP signaling displays regionalized activity within limb fetal muscles at

the muscle and tendon interface level, and fetal MPCs respond to BMP signaling in chicken limbs (Wang et al., 2010), suggesting the appositional growth of limb muscles that is maintained by direct signaling from BMP-expressing tendons. Consistent with this, BMP signaling has been recently shown to promote mesoderm-derived fibroblast transdifferentiation into myoblasts and their incorporation within fetal muscle fibers at the muscle–tendon interface (Esteves de Lima et al., 2021). However, there is a lack of formal proof for whether BMPs act directly on developing limb muscle (thereby activating a BMP-dependent cell-autonomous response), at which developmental stage this interaction takes place, whether it involves BMPs in physiological signaling in orthotopic positions and whether this impacts muscle patterning.

BMPs signal on target cells via transmembrane serine/threonine kinase receptors, which form a ligand-receptor complex that permits the phosphorylation of the type I receptor via the constitutively active type II receptor (Nohe et al., 2002, 2004). The type I receptor in turn phosphorylates the BMP-responsive R-SMAD proteins 1, 5 and 9 (pSMAD1/5/9), which subsequently form complexes with co-SMAD4 and translocate into the nucleus to regulate transcriptional activity of target genes (Miyazawa and Miyazono, 2017). Upon BMP signaling, the inhibitory SMAD6 becomes upregulated as part of a negative feedback loop. SMAD6 interferes with BMP signaling by blocking R-SMAD phosphorylation at the level of the receptor, by antagonizing the pSMAD1/co-SMAD4 complex formation, and by increasing ubiquitin-mediated proteolysis of the BMP signaling components (Goto et al., 2007; Hata et al., 1998; Murakami et al., 2003).

Here, we explored the role of BMP signaling during mouse limb muscle development. We employed overexpression of human

*SMAD6* (*huSMAD6*) as a mean to cell-autonomously interfere with BMP signaling. We overexpressed *huSMAD6* in embryonic limb MPCs and differentiated limb muscles following Cre-induced recombination by crossing of *Rosa26<sup>LoxP-Stop-LoxP-huSMAD6-IRES-EGFP</sup>* mice with Cre-driver mouse lines *Lbx1<sup>Cre</sup>* and *HSA-Cre* (Miniou et al., 1999; Sieber et al., 2007; Stantzou et al., 2017).

## RESULTS

### BMP signaling is active in limb muscle progenitors

First, we identified whether limb myogenic cells respond to BMP signaling. We monitored the nuclear accumulation of BMP-induced phosphorylated SMAD proteins using double immunofluorescence against pSMAD1/5/9 (pSMADs) and myogenic markers in mouse forelimbs at different developmental stages. In E10.5 limb buds, migrating MPCs expressed the transcription factor PAX3 (Fig. 1), whereas the PAX7 and MYOD transcription factors were not detected, thus reproducing previously published data (Lepper and Fan, 2010; Wood et al., 2013). Surprisingly, all PAX3<sup>+</sup> MPCs accumulated high levels of pSMADs, whereas non-myogenic mesenchymal cells showed no or, if any, very weak levels of pSMADs (Fig. 1). One day later, at E11.5, PAX3<sup>+</sup> MPCs rapidly lost BMP signaling responsiveness during lineage progression. Emerging MYOD<sup>+</sup> cells showed pSMADs in varying levels, some were negative and others showed a continuum from faintly to strongly positive. PAX7<sup>+</sup> cells, however, were rarely pSMAD<sup>+</sup> (Fig. 1). Of note, pSMAD<sup>+</sup> non-myogenic cells were also found in the progress zone of E11.5 limb buds (Fig. 1).

By the end of the embryonic period, at E14.5, pSMADs were enriched at the tips of the muscle fibers abutting tendons (Fig. S1A). Double labeling of pSMADs with either PAX7, MYOD or myosin

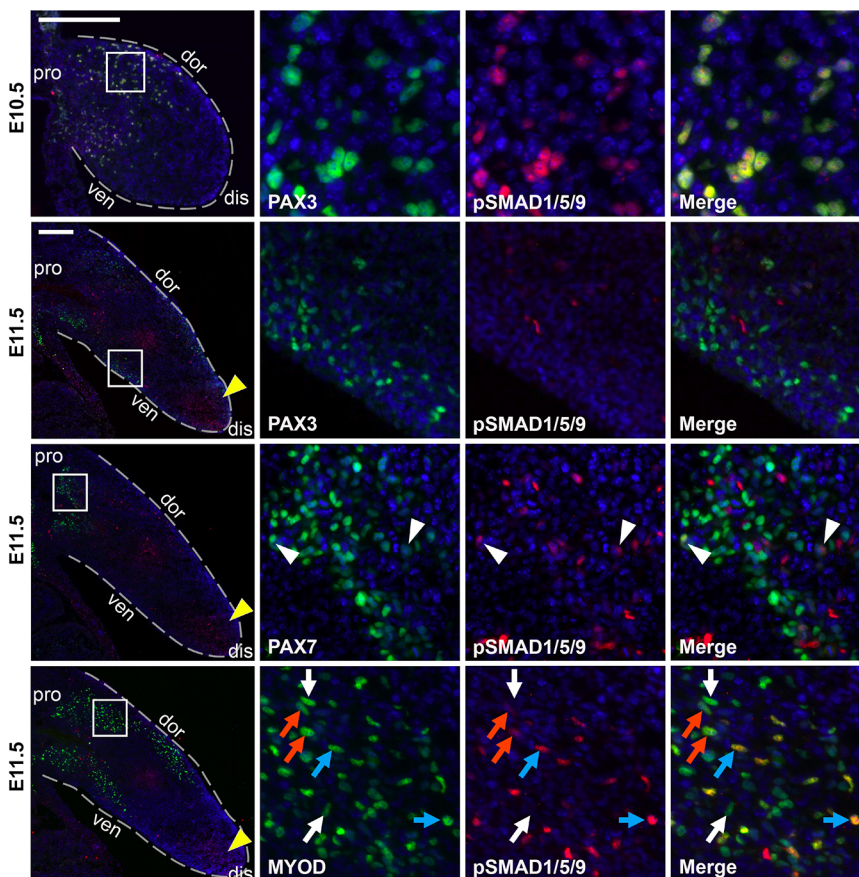


**Fig. 1. BMP signaling activity in developing limbs.**

Longitudinal sections of E10.5 and E11.5 forelimbs depict immunofluorescence signal of pSMAD1/5/9 (red) and PAX3, PAX7 or MYOD (green) following co-immunohistochemistry. Nuclei are stained with DAPI (blue). Left images show entire forelimbs, which are outlined by dashed lines. Insets (right) show magnification of boxed areas and depict individual and merged fluorescence channels. White arrowheads show the few PAX7<sup>+</sup> cells positive for pSMAD1/5/9. MyoD<sup>+</sup> cells negative for pSMAD1/5/9 are depicted with white arrows, faintly positive ones with orange arrows, strongly positive ones with light blue arrows. Yellow arrowheads depict pSMAD1/5/9 expression in the progress zone of E11.5 limb buds. *n*=5 biological replicates for each immunostaining and embryonic stage. dis, distal; dor, dorsal; pro, proximal; ven, ventral. Scale bars: 200  $\mu$ m.

heavy chain (MHC) antibodies showed active BMP signaling in MYOD<sup>+</sup> myonuclei at the myotendinous junctions and notably not in tendons (Fig. S1A). Low levels of pSMADs were also detected in rare PAX7<sup>+</sup> MPCs at the muscle tips (Fig. S1A). This confirms, in mouse, the presence of BMP-responsive myonuclei and MPCs at the tips of primary myofibers facing tendons, reminiscent of previous work in chick (Esteves de Lima et al., 2021).

By the end of the fetal period, at E18.5, the pSMAD expression pattern was reversed. Indeed, the tips of fetal muscle fibers were devoid of pSMADs, which had now accumulated in the nuclei of non-muscle cells at the muscle–tendon interface (Fig. S1A). MCT cells, labeled by the marker TCF4, were rarely pSMAD<sup>+</sup> (Fig. S1B). Furthermore, PAX7<sup>+</sup> and MYOD<sup>+</sup> myogenic cells occasionally accumulated pSMADs (Fig. S1B), consistent with the role of BMP signaling in postnatal satellite cells (Stantzou et al., 2017).

### MPCs maintain myogenic fate following abrogation of BMP signaling

We abrogated BMP signaling in limb MPCs by crossing *Lbx1*<sup>Cre</sup> mice (Sieber et al., 2007) with *Rosa26*<sup>LoxP-Stop-LoxP-huSMAD6-IRES-EGFP (*RS6*) animals (Stantzou et al., 2017). In the resulting *Lbx1*<sup>Cre</sup>;*RS6* embryos, activation of the *Lbx1* promoter in migrating limb MPCs induced Cre-mediated excision of the *LoxP-Stop-LoxP* cassette, leading to the expression of the inhibitory human *SMAD6* (*huSMAD6*) and enhanced green fluorescent protein (EGFP). The *Lbx1*<sup>Cre</sup>;*RS6* genotype was detected at the expected frequency up to the fetal stages. However, new-born *Lbx1*<sup>Cre</sup>;*RS6* mice rarely survived, and the very few that did had severe growth retardation (Fig. S10A). We validated the activation of the transgenes in *Lbx1*<sup>Cre</sup>;*RS6* embryos using EGFP as a marker of successful recombination. EGFP fluorescence was detected in cells from the proximal central field of E10.5 forelimb buds and was absent from the *RS6* controls (Fig. 2A). When compared with whole mount *in situ* hybridization (WISH) against *Lbx1*, the position of the EGFP fluorescence corresponded to that of migrating MPCs that populated the limb mesenchyme (Fig. 2A). In the forelimb buds of E12.5 *Lbx1*<sup>Cre</sup>;*RS6* embryos, EGFP was present in areas corresponding to the position of premuscle masses, as indicated by *Myod* (also known as *Myod1*) mRNA expression (Fig. 2A).</sup>

As the EGFP fluorescence was quite weak after cryosectioning, we used *Ai9* mice, a Cre recombinase-dependent tandem dimer Tomato (tdTomato) reporter strain (Madisen et al., 2010), to generate *Lbx1*<sup>Cre</sup>;*RS6*/*LoxP-Stop-LoxP-tdTomato* (*Lbx1*<sup>Cre</sup>;*RS6*/*Ai9*) embryos. All tdTomato<sup>+</sup> MPCs were also positive for EGFP and for PAX3, allowing the tracing of limb MPCs, which were depleted of BMP signaling during limb mesenchyme invasion (Fig. 2B). We did not find any tdTomato<sup>+</sup>/EGFP<sup>+</sup> MPC accumulation in somites at limb level, nor aberrant migration into the anterior/posterior/distal limb margins (Fig. 2B). At E18.5, there was strong EGFP and tdTomato fluorescence in the limb muscles of *Lbx1*<sup>Cre</sup>;*RS6*/*Ai9* fetuses (Fig. 2C). TdTomato was present in all myofibers of E18.5 forelimbs, indicating high recombination efficiency (Fig. 2C). TdTomato expression was observed exclusively in developing muscles, indicating that MPCs depleted of BMP activity differentiated exclusively into muscle cells (Fig. 2C).

As *Lbx1*<sup>Cre</sup> represents a loss-of-function allele due to insertion of the *Cre* transgene into the *Lbx1* exon 1 coding sequence (Sieber et al., 2007), we determined whether heterozygous *Lbx1*<sup>Cre</sup> mice show signs of haploinsufficiency. Myogenic marker WISH revealed a similar expression pattern in *Lbx1* and *Pax3* at E10.5 or *Myod* at E11.5 in *Lbx1*<sup>Cre</sup> limbs compared with that in the *RS6* controls

(Fig. S10B). Furthermore, the *Lbx1*<sup>Cre</sup> mice had normal viability and reproduction rates. We concluded that the loss of one functional *Lbx1* allele did not cause haploinsufficiency, allowing us to use *RS6* and *Lbx1*<sup>Cre</sup> as controls for experiments with *Lbx1*<sup>Cre</sup>;*RS6* mutants.

In summary, these results show that following Cre-recombination, the *huSMAD6-IRES-EGFP* cassette was expressed exclusively in MPCs and their progeny in developing limbs of *Lbx1*<sup>Cre</sup>;*RS6* mice, allowing permanent overexpression of the BMP signaling inhibitor SMAD6 in cells of the myogenic lineage.

### *huSMAD6* overexpression abrogates BMP signaling and downregulates the marker genes of limb muscle development

We confirmed via RT-qPCR that *huSMAD6* was upregulated (3.7-fold) in the E18.5 forelimb muscles of *Lbx1*<sup>Cre</sup>;*RS6* fetuses compared with that of the *RS6* controls (Fig. 2D). Next, we determined whether *huSMAD6* overexpression caused cell-autonomous abrogation of BMP signaling in the myogenic lineage. Indeed, we observed the absence of pSMADs in PAX3<sup>+</sup> MPCs in E10.5 *Lbx1*<sup>Cre</sup>;*RS6* limb buds compared with the *RS6* controls (Fig. 3A). In addition, the presence of pSMADs at the tips of E14.5 muscle fibers was also lost (Fig. 3B). Moreover, WISH revealed that *Lbx1* and *Pax3* expression was strongly reduced in E10.5 *Lbx1*<sup>Cre</sup>;*RS6* limb buds compared with that in the *RS6* controls (Fig. 3C). Residual *Lbx1* and *Pax3* transcripts were found in the proximal part of the limb buds. Similarly, *Myod* expression was strongly reduced in E11.5 and E12.5 limb buds from *Lbx1*<sup>Cre</sup>;*RS6* embryos compared with that from the *RS6* controls (Fig. 3C). However, using WISH, we were unable to discriminate whether the decreased gene expression was due to a decrease in cell number or in the transcript number per cell.

### Abrogation of BMP signaling dampens limb MPC proliferation and distal migration

We transversely cryosectioned E10.5 embryos at limb level, allowing for a proximodistal sectioning plane of the developing limb bud. Double immunofluorescence for PAX3 and the proliferation marker KI67 revealed ~40% reduction of the entire PAX3<sup>+</sup> cell population and a decline in the PAX3<sup>+</sup>/KI67<sup>+</sup> subpopulation in *Lbx1*<sup>Cre</sup>;*RS6* embryos, suggesting reduced MPC proliferation after the inhibition of BMP signaling (Fig. 4A–C). The cell death marker cleaved Caspase-3 was absent in E10.5 limb mesenchyme in both genotypes, whereas it was present at trunk level and, as expected, at interdigital positions of E12.5 autopods (Fig. S2A). In addition, we analyzed the proximodistal distribution of the PAX3<sup>+</sup> cell population in the E10.5 limb buds and found that total cell numbers were significantly reduced in the middle and distal parts of the limb bud in *Lbx1*<sup>Cre</sup>;*RS6* embryos compared with that in the *RS6* controls (Fig. 4D,E). As total PAX3<sup>+</sup> cell number in *Lbx1*<sup>Cre</sup>;*RS6* limbs was lower than in *RS6* limbs, we also analyzed the normalized distribution of PAX3<sup>+</sup> cells along the proximodistal axis. Such analysis revealed a decreased presence of normalized PAX3<sup>+</sup> cell numbers in the distal parts of the limb, whereas there was a tendency towards increased cell numbers in the proximal parts (Fig. S2B). Next, we determined the distribution of PAX3<sup>+</sup> cell in dorsal and ventral premuscle masses. We found a ~40% reduction in cell numbers within the dorsal and ventral premuscle masses when comparing *Lbx1*<sup>Cre</sup>;*RS6* limbs with *RS6* limbs (Fig. S2C), which accords with the loss in total PAX3<sup>+</sup> cell number in *Lbx1*<sup>Cre</sup>;*RS6* limbs (compare with Fig. 4B). Cell numbers, however, were similar when comparing dorsal and ventral muscle masses of the same genotype (Fig. S2C). Together, these data suggest that the

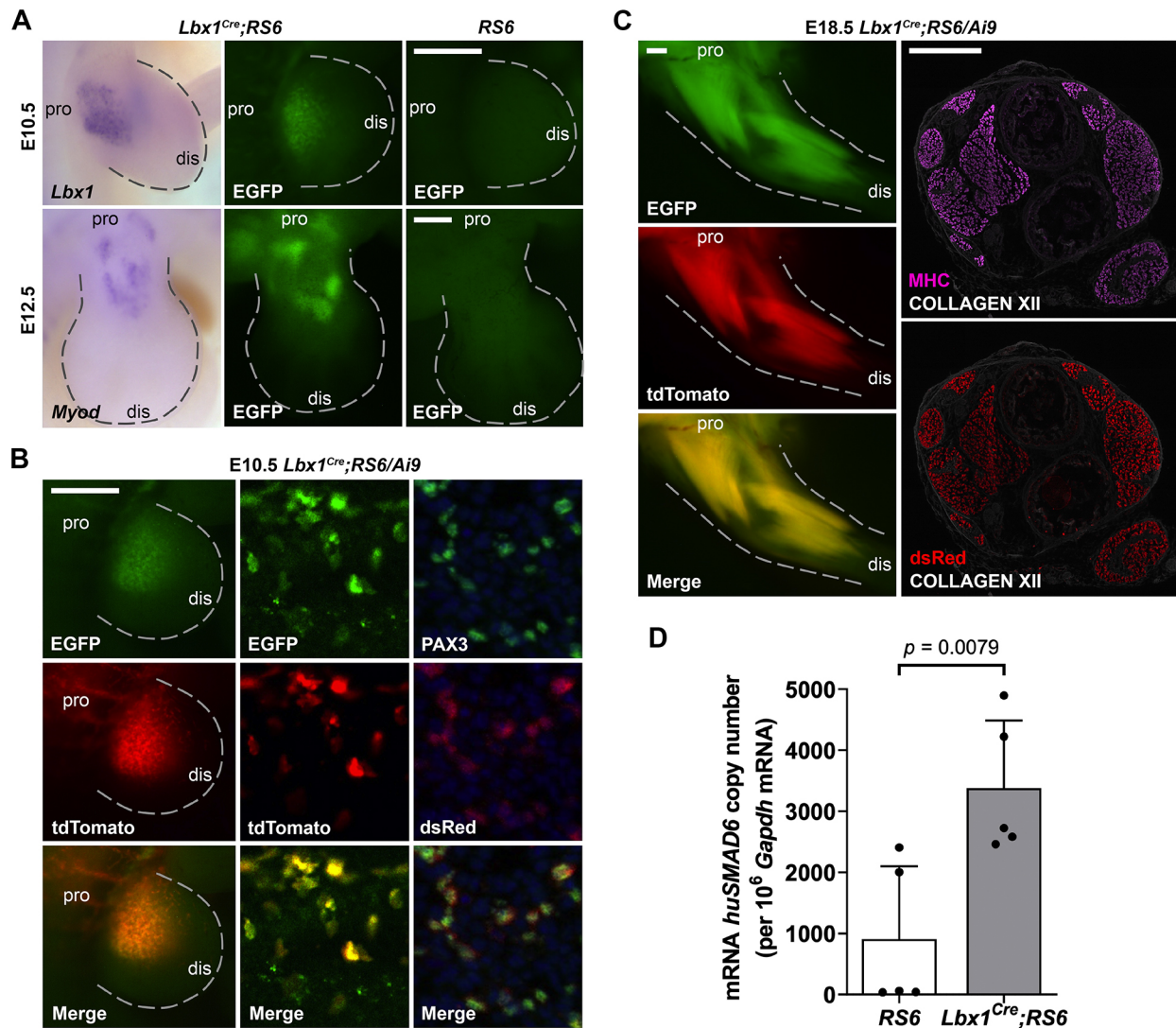


**Fig. 2. Fate mapping of limb MPCs.** (A) Images depict the dorsal view of forelimbs (outlined by dashed lines), where there is native EGFP fluorescence (green) in recombined cells from E10.5 and E12.5 forelimbs from *Lbx1<sup>Cre</sup>;RS6* mice (right) compared with the position of pre-muscle masses as revealed by *Lbx1* and *Myod* transcripts (purple) following WISH (left).  $n=5$  biological replicates for each condition. (B) Dorsal view of an E10.5 limb bud (outlined by dashed lines) of *Lbx1<sup>Cre</sup>;RS6/Ai9* embryos depicts native fluorescence of EGFP (green) and tdTomato (red) at low magnification (left column) and at higher magnification (middle column). The right column depicts co-immunostaining for PAX3 (green) and DsRed (red) on cryosections of E10.5 *Lbx1<sup>Cre</sup>;RS6/Ai9* forelimbs. Nuclei are stained with DAPI (blue).  $n=5$  biological replicates for each condition and genotype. (C) Left images depict dorsal view of an E18.5 forelimb (outlined by dashed lines) of an *Lbx1<sup>Cre</sup>;RS6/Ai9* fetus showing native fluorescence of EGFP (green) and tdTomato (red) in the limb muscles. The right images depict co-immunostaining for MHC (magenta), collagen type 12 (white) and tdTomato (red) in transverse sections of forelimbs at zeugopod level.  $n=5$  biological replicates for each condition/immunostaining. (D) Dot-plotted bar graph shows the relative quantified mRNA expression of *huSMAD6* per 1 million *Gapdh* mRNA in E18.5 forelimb muscles in *RS6* and *Lbx1<sup>Cre</sup>;RS6* fetuses using RT-qPCR.  $n=5$  biological replicates. Data are mean+s.d.  $P$ -value calculated using non-parametric two-tailed Mann–Whitney  $U$ -test. dis, distal; pro, proximal. Scale bars: 500  $\mu$ m.

lack of BMP signaling in MPCs attenuated their proliferation and distal migration, and argue against a loss of MPCs by apoptosis or a rerouting of migration.

#### Abrogation of BMP signaling accelerates myogenesis progression of limb MPCs

In the embryonic limb, PAX3 controls the entry of MPCs into the myogenic program (Relaix et al., 2005; Lagna et al., 2008). In E11.5 *RS6* forelimbs, we observed a transition from PAX3 to PAX7 and MYOD expression. PAX7<sup>+</sup> cells emerged in proximal pre-muscle masses (Fig. 5A). PAX3<sup>+</sup> cells were located closer to the ectoderm, whereas MYOD<sup>+</sup> cells were present closer to the

core of the limb bud (Fig. 5B), consistent with the myogenic lineage progression from the peripheral towards central limb mesenchyme observed in developing chicken limbs (Amthor et al., 1998).

We found a precocious conversion of PAX3<sup>+</sup> cells towards PAX7<sup>+</sup> and MYOD<sup>+</sup> cells in E11.5 *Lbx1<sup>Cre</sup>;RS6* limbs: the total number of PAX3<sup>+</sup> cells decreased by 85%, whereas the total number of PAX7<sup>+</sup> cells increased by 64% and the MYOD<sup>+</sup> cells by 46% (Fig. 5A–E), thus the total PAX3/PAX7/MYOD population remained stable. In addition, the PAX3<sup>-</sup>/PAX7<sup>+</sup> and PAX3<sup>-</sup>/MYOD<sup>+</sup> cell population ratios increased by 68% and 61%, respectively, compared with that in the *RS6* controls (Fig. 5F,G).

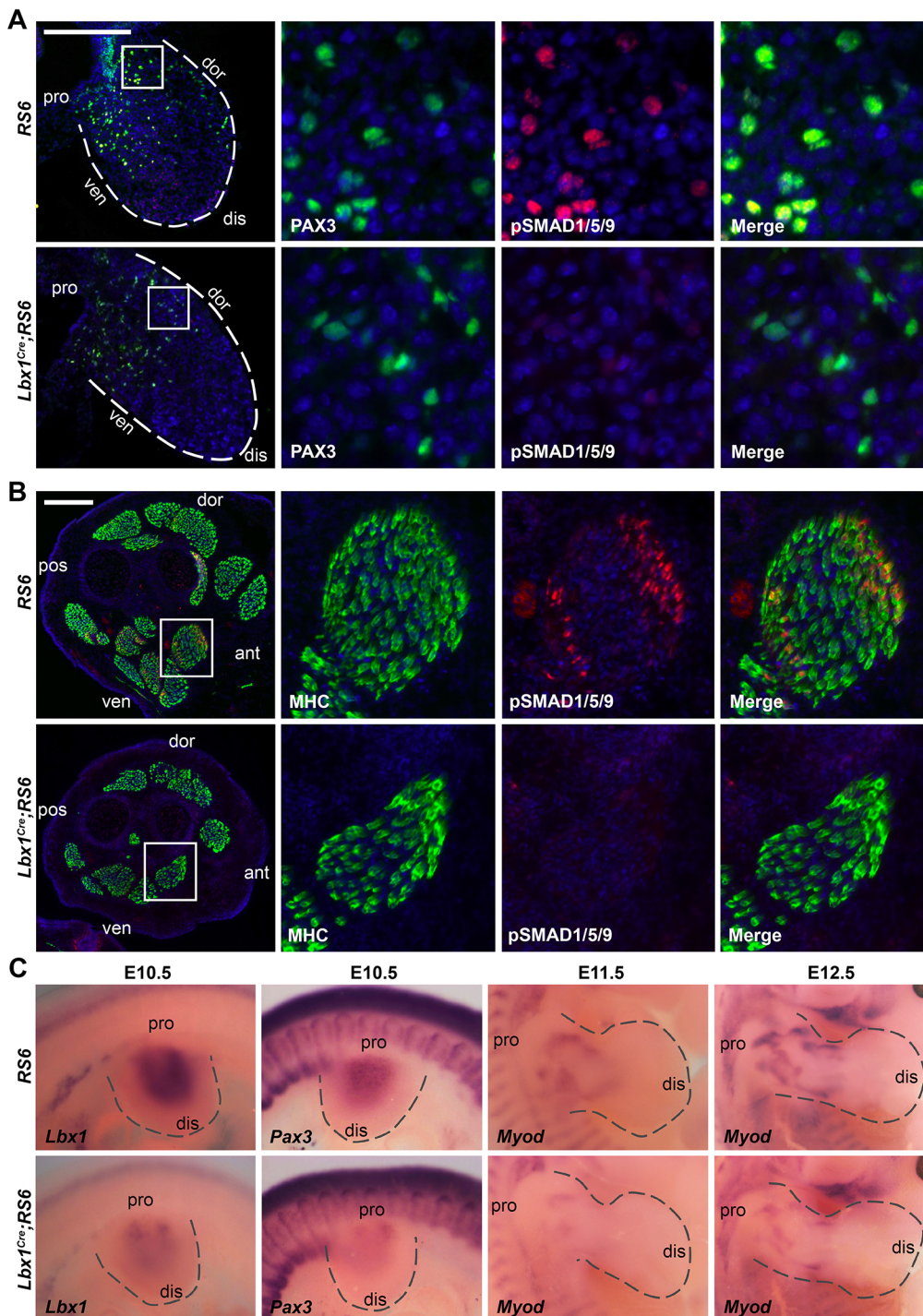


**Fig. 3. Effect of *huSMAD6* overexpression in the developing limb muscles.** (A,B) Effect of *huSMAD6* overexpression on BMP signaling. (A) Left images depict the immunofluorescence signals of PAX3 (green) and pSMAD1/5/9 (red) following co-immunohistochemistry on longitudinal sections of E10.5 entire forelimbs of *RS6* and *Lbx1<sup>Cre</sup>;RS6* embryos. Nuclei are stained with DAPI (blue). Forelimbs are outlined by dashed lines. Insets (right) show magnification of boxed areas and depict individual and merged fluorescence channels. (B) Left images depict immunofluorescence signals of MHC (green) and pSMAD1/5/9 (red) following co-immunohistochemistry on transverse sections at mid-zeugopod level of E14.5 forelimbs of *RS6* and *Lbx1<sup>Cre</sup>;RS6* embryos. Nuclei are stained with DAPI (blue). Insets (right) show magnification of boxed areas and depict the pronator teres muscle in individual and merged fluorescence channels.  $n=5$  biological replicates for all stages and immunostaining. (C) Effect of *huSMAD6* overexpression on the transcription of early markers of limb muscle development. The images show the expression patterns of *Lbx1*, *Pax3* and *Myod* transcripts (purple) following WISH of E10.5, E11.5 and E12.5 *Lbx1<sup>Cre</sup>;RS6* embryos compared with *RS6* controls. Images show dorsal view of the forelimbs (outlined by dashed line). ant, anterior; dis, distal; dor, dorsal; pos, posterior; pro, proximal; ven, ventral. Scale bars: 200  $\mu$ m in A,B.

These results suggest accelerated myogenic lineage progression in *Lbx1<sup>Cre</sup>;RS6* MPCs due to the absence of BMP signaling, which is similar to that shown in embryonic chicken limbs (Amthor et al., 1998).

In E12.5 *Lbx1<sup>Cre</sup>;RS6* limbs, the accelerated lineage progression was associated with a loss in total number of MYOD<sup>+</sup> cells (42%) and PAX7<sup>+</sup> cells (47%) (Fig. S3A-D). Furthermore, we detected a decline in PAX7<sup>+</sup>/KI67<sup>+</sup> and PAX7<sup>+</sup>/MYOD<sup>+</sup> cell populations, whereas the proportion of MYOD<sup>+</sup>/MYOG<sup>+</sup> cells increased, confirming the shift of myogenic lineage progression towards differentiating myoblasts at the expense of proliferating precursors (Fig. S3B,E-G).

### Abrogation of BMP signaling in MPCs disturbs *Lbx1<sup>Cre</sup>;RS6* limb proximodistal muscle patterning

We analyzed the consequences of decreased MPC generation on primary myofiber formation after abrogation of BMP signaling by visualizing myofibers on transverse sections at the end of the embryonic period (E14.5) of mouse forelimb development. The zeugopod muscles of *Lbx1<sup>Cre</sup>;RS6* embryos were significantly smaller and contained about half the number of primary myofibers compared with the *RS6* controls (Fig. 6). At this stage, we observed defective muscle patterning in the *Lbx1<sup>Cre</sup>;RS6* embryos. Whereas muscle pattern was normal at stylopod level, certain zeugopod

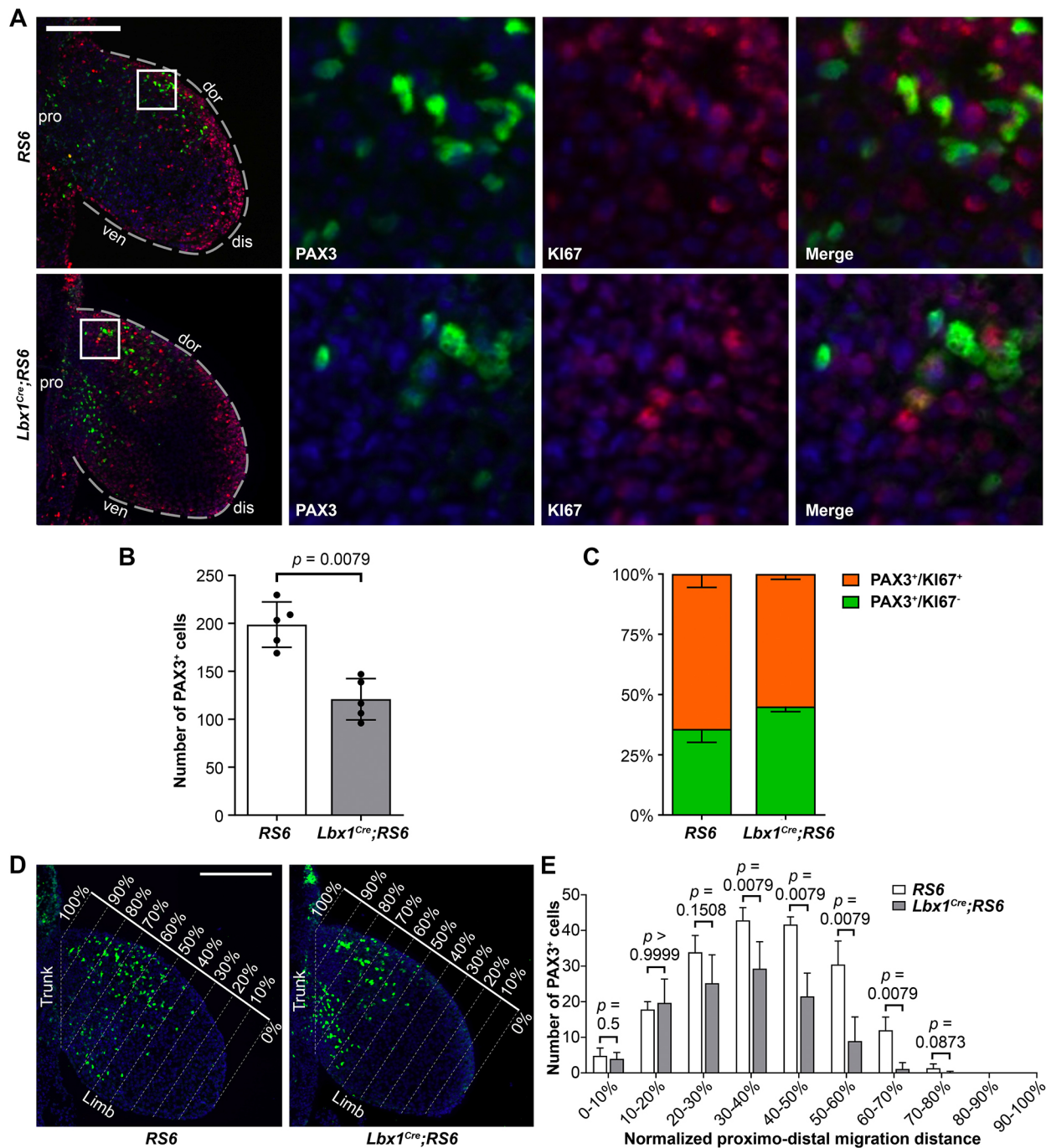


**Fig. 4. Effect of *huSMAD6* overexpression on limb MPC proliferation and migration.** (A) Left images depict immunofluorescence staining of PAX3 (green) and KI67 (red) following co-immunohistochemistry on longitudinal sections of E10.5 entire forelimbs (outlined by dashed line) of *RS6* control and *Lbx1<sup>Cre</sup>;RS6* embryos. Nuclei are stained with DAPI (blue). Insets (right) show magnification of boxed areas and depict individual and merged fluorescence channels. (B) Dot-plotted bar graph shows the number of PAX3<sup>+</sup> cells in the forelimbs of both genotypes. The number of cells was determined as average from three consecutive longitudinal sections. (C) Stacked bar graph depicts the percentages of PAX3<sup>+</sup>/KI67<sup>+</sup> (orange) ( $P=0.0079$ ) and PAX3<sup>+</sup>/KI67<sup>-</sup> (green) ( $P=0.0079$ ) MPCs in the forelimbs of both genotypes. (D) Immunofluorescence staining of PAX3 (green) and DAPI (blue) on longitudinal sections of E10.5 forelimbs of *RS6* control and *Lbx1<sup>Cre</sup>;RS6* embryos. The limb was divided into ten equal zones along the proximodistal axis. (E) Histogram depicts the number of PAX3<sup>+</sup> MPCs based on their position along the proximodistal limb axis as depicted in D.  $n=5$  biological replicates for each genotype. Each replicate represents the mean of three consecutive serial sections. Data are mean $\pm$ s.d.  $P$ -values calculated using non-parametric two-tailed Mann–Whitney  $U$ -test. dis, distal; dor, dorsal; pro, proximal; ven, ventral. Scale bars: 200  $\mu$ m.

muscles were either completely absent (supinator, extensor pollicis, flexor digitorum superficialis) or fused (extensor carpi radialis longus and brevis), whereas the remaining zeugopod muscles were remarkably hypoplastic (Fig. 6). At the autopod level, only a few

remnant MHC-expressing cells were observed, and autopod muscles were entirely absent (Fig. 6). The anatomical changes in muscle pattern seen at the end-embryonic stage (E14.5) persisted during the fetal stage (Fig. 7).

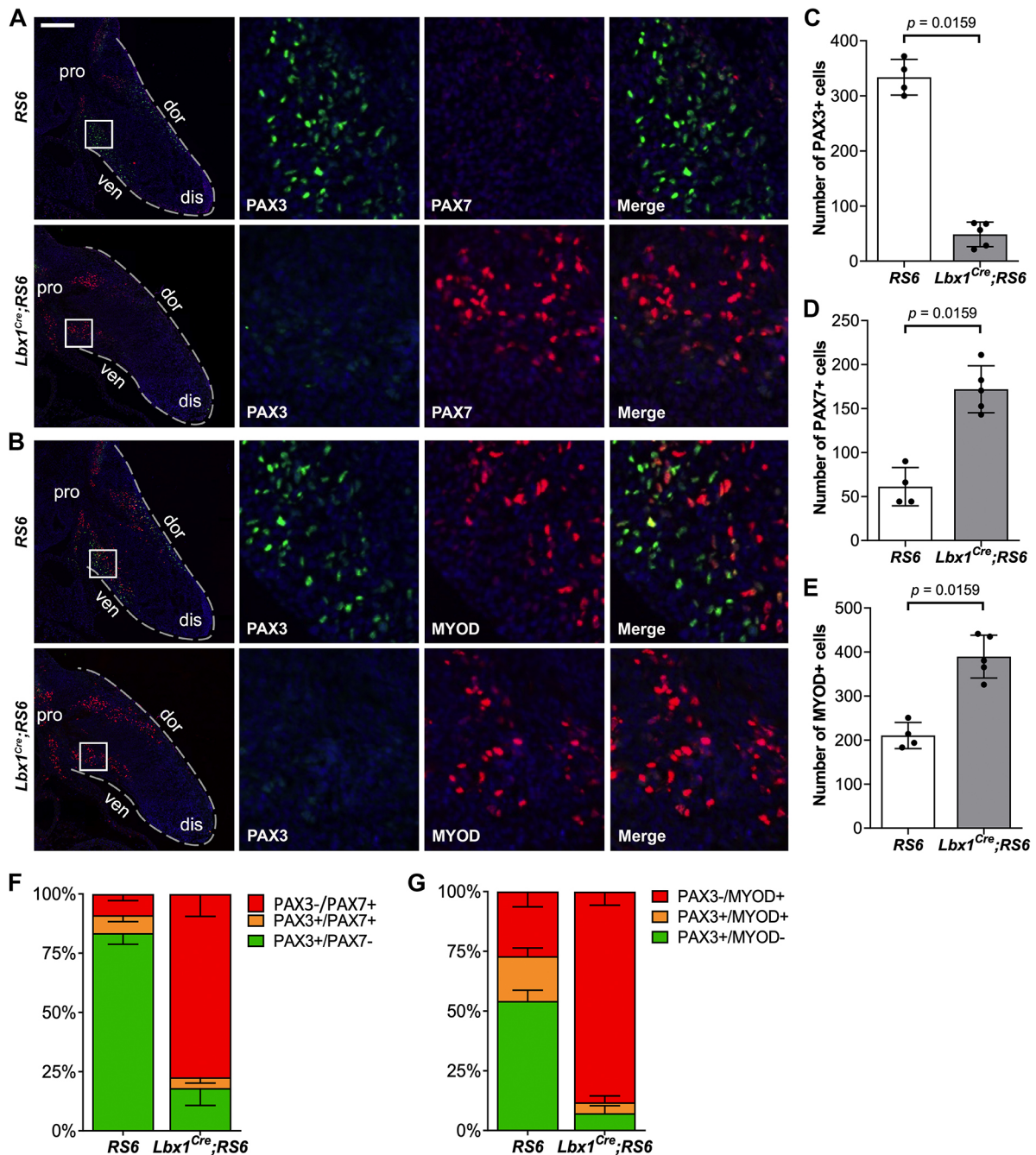


**Fig. 5. Effect of *huSMAD6* overexpression on myogenic lineage progression.** (A,B) Left images depict immunofluorescence staining of PAX3 (green) and either PAX7 or MYOD (red) after co-immunohistochemistry on longitudinal sections of E11.5 entire forelimbs of RS6 control and *Lbx1<sup>Cre</sup>;RS6* embryos. Nuclei are stained with DAPI (blue). Limbs are outlined by dashed lines. Insets (right) show magnification of boxed areas and depict individual and merged fluorescence channels. (C-E) Dot-plotted bar graphs show the total number of PAX3<sup>+</sup> (C), PAX7<sup>+</sup> (D) and MYOD<sup>+</sup> (E) cells. (F) Stacked bar graph depicts the percentages of PAX3<sup>+</sup>/PAX7<sup>-</sup> cells (green) (*P*=0.0159), PAX3<sup>+</sup>/PAX7<sup>+</sup> cells (orange) (*P*=0.1905) and PAX3<sup>-</sup>/PAX7<sup>+</sup> cells (red) (*P*=0.0159). (G) Stacked bar graph depicts the percentages of PAX3<sup>+</sup>/MYOD<sup>-</sup> cells (green) (*P*=0.0159), PAX3<sup>+</sup>/MYOD<sup>+</sup> cells (orange) (*P*=0.0159) and PAX3<sup>-</sup>/MYOD<sup>+</sup> cells (red) (*P*=0.0159) cells. *n*=4 biological replicates for RS6 and *n*=5 for *Lbx1<sup>Cre</sup>;RS6*. Each replicate represents the mean of three consecutive serial sections. Data are mean±s.d. *P*-values calculated using non-parametric two-tailed Mann–Whitney *U*-test. dis, distal; dor, dorsal; pro, proximal; ven, ventral. Scale bar: 200 μm.

### Normal muscle patterning following abrogation of BMP signaling in differentiated muscle

We wanted to determine whether defective muscle patterning was also caused by the abrogation of BMP signaling in differentiated muscle cells. We used *HSA-Cre* driver mice to conditionally direct recombination in differentiated muscle cells. We first performed a

time course to determine the spatiotemporal occurrence of HSA-Cre-driven recombination in *HSA-Cre;Ai9* crosses by following the onset of tdTomato expression. In E10.5 and E11.5 embryos, tdTomato was found in somites but not in limb buds. TdTomato was present in developing limb muscles from E12.5 onwards, which is consistent with the emergence of primary myofibers at this stage (Fig. S4). We then

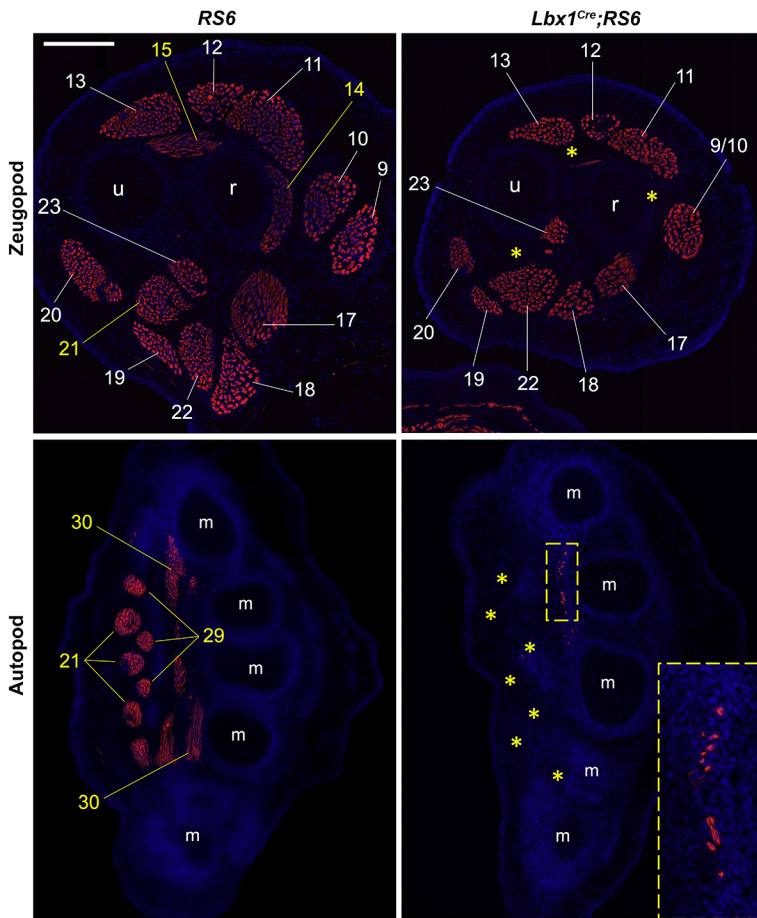


**Fig. 6. Effect of *huSMAD6* overexpression on embryonic muscle pattern.** Immunostaining for MHC (red) on transverse sections at the zeugopod (upper images) and autopod (lower images) level of E14.5 forelimbs from *RS6* and *Lbx1<sup>Cre</sup>;RS6* embryos. Nuclei are stained with DAPI (blue). Inset (yellow dashed lines) shows magnification of boxed area and depicts remnants of MHC-expressing cells in the *Lbx1<sup>Cre</sup>;RS6* forelimb autopod. Muscles that are numbered in yellow in *RS6* embryos, are absent from the *Lbx1<sup>Cre</sup>;RS6* embryos (yellow asterisks). Letters indicate the bones: m, metacarpals; r, radius; u, ulna. Numbers indicate the muscles: 9, extensor carpi radialis longus; 10, extensor carpi radialis brevis; 11, extensor digitorum communis; 12, extensor digitorum lateralis; 13, extensor carpi ulnaris; 14, supinator; 15, extensor pollicis; 16, extensor indicis proprius; 17, pronator teres; 18, flexor carpi radialis; 19, palmaris longus; 20, flexor carpi ulnaris; 21, flexor digitorum superficialis; 22/23/24/25, flexor digitorum profundus (superficial 's', humeral 'h', ulnar 'u' and radial 'r' heads); 26, pronator quadratus; 27, thenars; 28, hypothenars; 29, lumbricals; 30, interossei.  $n=5$  biological replicates. Scale bar: 200  $\mu$ m.

generated *HSA-Cre;RS6* mice to overexpress *huSMAD6* exclusively in terminally differentiated muscles; a mouse model we have validated previously (Stantzou et al., 2017). The forelimbs of E18.5 *HSA-Cre;RS6* fetuses developed normally and no change was detected in the muscle pattern (Fig. 7). These results may indicate that the information for the future muscle pattern is already present in MPCs before their differentiation. An alternative explanation may be that sufficient MPCs reached their destination (as migration and/or proliferation were not affected), allowing them to be exposed to patterning cues. Of note, MCT did not increase at the expense of skeletal muscle, as the pattern of collagen 12 expression in the *HSA-Cre;RS6* fetuses was similar to that of the controls despite the smaller muscles (Fig. 7).

### BMP signaling impacts Hox expression of myogenic cells

The observed changes in the muscle pattern of *Lbx1<sup>Cre</sup>;RS6* mutants (Fig. 7) resembled those previously observed in *Hoxa11/d11* double mutants (Swinehart et al., 2013), raising the question of the intrinsic positional information of myogenic cells and putative regulation by BMP signaling.

Indeed, at E10.5, *PAX3<sup>+</sup>* MPCs, which had left the dermomyotome and migrated into the limb bud, expressed *HOXA11* protein. Notably, *HOXA11* levels in the MPCs were higher than in the surrounding limb mesenchymal cells (Fig. 8A). As early as 1 day later, at E11.5, most *PAX3<sup>+</sup>* cells had lost the high *HOXA11* protein levels (Fig. 8B). In the absence of BMP signaling in *Lbx1<sup>Cre</sup>;RS6* embryonic limbs, the MPCs failed to accumulate high levels of *HOXA11* protein (Fig. 8C compared with 8A; Fig. S5A).

To gain a global vision of Hox gene expression at single-cell resolution, we analyzed open-access single-cell RNA-sequencing

(scRNA-seq) datasets of early chicken and mouse whole limb buds (Esteves de Lima et al., 2021; Rouco et al., 2021). Chicken and mouse limb buds have comparable Hox patterns in limb mesenchyme and myogenic differentiation (Pownall et al., 2002; Sundin et al., 1990; Yakushiji-Kaminatsui et al., 2018).

In chicken forelimb buds, scRNA-seq showed the expression of genes of the *HOXA* and *HOXD* clusters in mesenchymal cells and in muscle cluster cells (Figs S5B-H and S6). As an example, *HOXA11* transcripts were detected in the majority (69%) of muscle cluster cells in E4 limbs (E10.5 mouse stage equivalence) and more rarely (37% of cells) by E6 (E12.5 mouse stage equivalence). In contrast, *HOXD13* transcripts were not detected before E6, at which point its expression was limited to a few muscle cluster cells (Fig. S5B). *HOXA11* was expressed at all successive steps of the myogenic process: first in *PAX7<sup>+</sup>* and *MYOD<sup>+</sup>* MPCs at E4 and E6, and then in *MYOG<sup>+</sup>* myoblasts at E6 (Fig. S5C-G). There was nonetheless a drop in *HOXA11* expression during myogenic lineage progression, given that at E6, 39% of *PAX7<sup>+</sup>* muscle cluster cells co-expressed *HOXA11*, whereas only 15% of *MYOG<sup>+</sup>* cells co-expressed *HOXA11* (Fig. S5H). Interestingly, we found a heterogeneous combinatorial expression of *HOXA* genes in single muscle cluster cells, suggesting Hox-dependent positional information in chicken limb MPCs (Fig. S6A,B).

We next analyzed whether BMP response correlates with *HOXA* gene expression in muscle cluster cells and found that *HOXA<sup>+</sup>* cells (expressing one or several genes of the *HOXA* cluster) expressed BMP downstream effector genes *ID2* and *ID3*, but not *ID1*, in higher proportion compared with *HOXA<sup>-</sup>* cells (Fig. S6C-E). Consistently, the BMP score, which is the corrected average



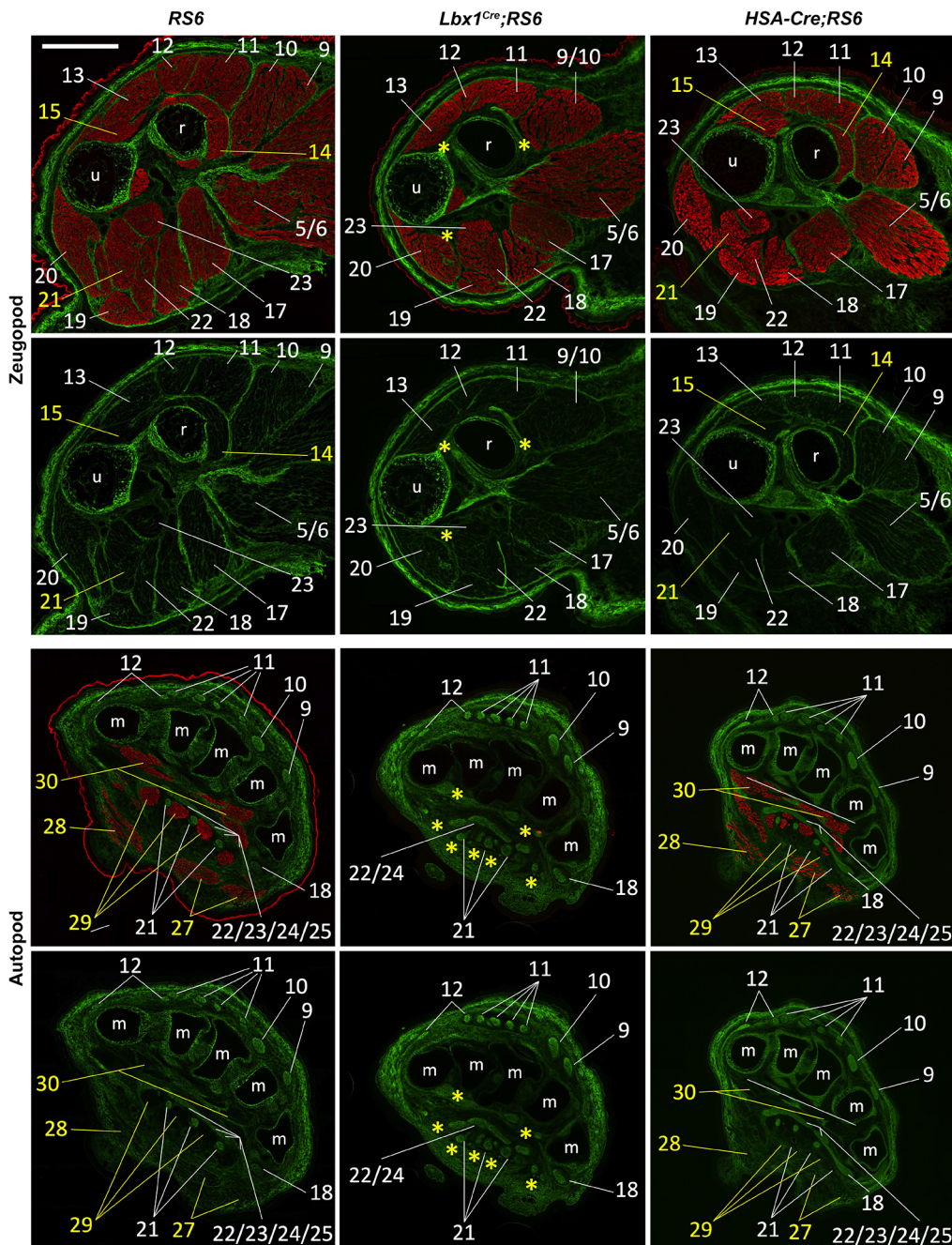


**Fig. 7. Effect of *huSMAD6* overexpression on fetal muscle pattern.** Immunostaining for MHC (red) and collagen 12 (green) on transverse sections at the zeugopod (upper images) and autopod (lower images) level of E18.5 forelimbs from *RS6*, *Lbx1<sup>Cre</sup>;RS6* and *HSA-Cre;RS6* embryos. Rows 1 and 3 show merged images; rows 2 and 4 show collagen 12. Muscles that are numbered in yellow in *RS6* embryos are absent from the *Lbx1<sup>Cre</sup>;RS6* embryos (yellow asterisks). Letters indicate the bones: m: metacarpals; r, radius; u, ulna. Numbers indicate muscles as well as the corresponding MCT compartments and tendons: 9, extensor carpi radialis longus; 10, extensor carpi radialis brevis; 11, extensor digitorum communis; 12, extensor digitorum lateralis; 13, extensor carpi ulnaris; 14, supinator; 15, extensor pollicis; 16, extensor indicis proprius; 17, pronator teres; 18, flexor carpi radialis; 19, palmaris longus; 20, flexor carpi ulnaris; 21, flexor digitorum superficialis; 22/23/24/25, flexor digitorum profundus (superficial 's', humeral 'h', ulnar 'u' and radial 'r' heads); 26, pronator quadratus; 27, thenars; 28, hypothenars; 29, lumbricals; 30, interossei.  $n=5$  biological replicates. Scale bar: 500  $\mu$ m.

expression of the *ID1*, *ID2* and *ID3* genes, was significantly higher in *HOXA*<sup>+</sup> cells compared with *HOXA*<sup>-</sup> cells (Fig. S6F).

scRNA-seq of E12.5 mouse forelimbs showed very similar results compared with those in chicken: (1) muscle cluster cells expressed genes of the *Hoxa* and *Hoxd* clusters (Fig. S7A); (2) a subset of *Hoxa11*<sup>+</sup> muscle cluster cells co-expressed *Pax3*, *Pax7*, *Myf5* and *Myod*, but only rarely *Myog* (Fig. S8); (3) muscle cluster cells showed large heterogeneity in the expression of genes of the *Hoxa* cluster (Fig. S7B); and (4) there was *Id1*, *Id2* and *Id3* expression in a higher proportion of *Hoxa*<sup>+</sup> cells than *Hoxa*<sup>-</sup> cells (Fig. S7C-E).

## DISCUSSION

The current paradigm of limb muscle patterning considers limb MPCs as naïve, where they develop individual muscles by invading a prepattern established by MCT (Kardon et al., 2003). Our results

contribute to this concept by showing that BMP signaling (produced by limb connective tissue cells surrounding developing muscles; Amthor et al., 1998; Esteves de Lima et al., 2021) is necessary for the generation of MPCs responsive to BMP, thereby establishing the necessary cellular source for limb muscle pattern. We used overexpression of *huSMAD6* as an experimental tool to abrogate BMP signaling, which caused precocious loss of PAX3 in MPCs and accelerated myogenic lineage progression. MPCs advanced less distally, as expected, as PAX3 is a prerequisite for myogenic migration (Bober et al., 1994), likely causing a mismatch between their distal progression and the local connective tissue, and thus responsible for the observed defects in proximodistal muscle pattern.

It has been shown that impaired distal MPC migration can cause varying degrees of limb muscle defects (Brohmann et al., 2000;

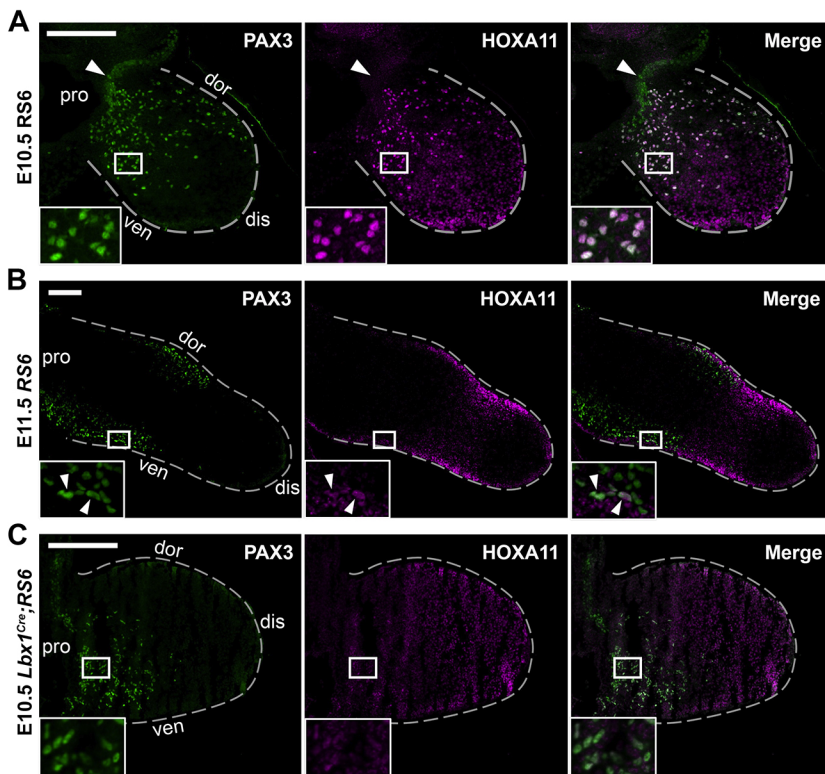


**Fig. 8. Hox proteins in MPCs rely on BMP signaling.**

(A–C) Co-immunohistochemistry of longitudinal sections of embryonic limbs. Forelimbs are outlined by dashed lines. Insets show magnifications of boxed areas and depict individual and merged fluorescence channels. (A) PAX3 (green) and HOXA11 (magenta) of control RS6 forelimbs at E10.5. Insets depict representative RS6 forelimb MPCs highly positive for HOXA11. White arrowheads indicate ventral lip of the dermomyotome. (B) PAX3 (green) and HOXA11 (magenta) of RS6 forelimbs at E11.5. Insets depict a portion of the mid-ventral pre-muscle mass. White arrowheads indicate the few PAX3<sup>+</sup> cell remaining positive for HOXA11. (C) PAX3 (green) and HOXA11 (magenta) of *Lbx1Cre*;RS6 forelimbs at E10.5. Insets depict representative *Lbx1Cre*;RS6 forelimb MPCs weakly positive for HOXA11. *n*=4–5 biological replicates for RS6 limbs and *n*=5 for *Lbx1Cre*;RS6 limbs. dis, distal; dor, dorsal; pro, proximal; ven, ventral. Scale bars: 200  $\mu$ m.

Shin et al., 2016; Vasyutina et al., 2005). A detailed anatomical analysis of these mouse mutants would be required to determine whether different signaling cues, e.g. scatter factor/hepatocyte growth factor (SF/HGF) as compared to BMPs, exert distinctive roles during muscle patterning. In the absence of such comparative anatomical analysis, however, we cannot exclude the possibility that migration defects, independently of the underlying molecular mechanisms, result in a generic patterning defect.

We demonstrated that limb MPCs expressed Hox genes in mouse as well as in chicken embryos. scRNA-seq revealed: (1) a high proportion of Hox-expressing MPCs in early limb buds; (2) heterogeneity of Hox gene expression in the MPCs; (3) their sequential upregulation; and (4) their downregulation during myogenic lineage progression. Immunohistochemistry confirmed the transcriptome data: upon leaving the dermomyotome and entering limb bud mesenchyme, PAX3<sup>+</sup> migrating limb MPCs produced high HOXA11 protein levels, and this was dependent on BMP signaling. Interestingly, the *Lbx1Cre*;RS6 mutants resembled the muscle pattern defect observed in *Hoxa11*<sup>-/-</sup>/*d11*<sup>-/-</sup> dKO mutants (Swinehart et al., 2013). Swinehart et al. showed that *Hoxa11* was not expressed by differentiated muscle cells at E14.5, but in cells surrounding primary muscle fibers, such as TCF4<sup>+</sup> connective tissue cells. Whether HOXA11 colocalizes with MPCs (which also surround primary muscle fibers), however, was not investigated (Swinehart et al., 2013). It has also been shown that *Hoxa13*<sup>-/-</sup> KO and *Hoxa13*<sup>-/-</sup>/*d13*<sup>-/-</sup> dKO disturb autopod development (Fromental-Ramain et al., 1996). Here, we found both *Hoxa13* and *Hoxd13* being expressed by MPCs. However, we examined scRNA-seq data sets from whole limb buds, which did not allow us to specify which MPC subpopulation (e.g. autopod MPCs) expressed which Hox code. Thus, it remains to be determined whether Hox gene expression in MPCs follows the collinearity in the developing limb. We can therefore only speculate about the exact role of Hox genes in developing muscle, and how

their expression relates to BMP signaling. Previous work on chick limb MPCs showed that *Hoxa11* and *Hoxd13* blocked expression of *MyoD*, and that Hox gain-of-function experiments resulted in distorted limb muscle patterning (Yamamoto and Kuroiwa, 2003). Many questions, however, remain unresolved. Does the Hox code control MPC proliferation, myogenic lineage progression and muscle splitting? Do MPCs, through Hox code, acquire positional identity and establish a muscle pre-pattern? Alternatively, herein observed loss in specific muscles may simply result from a tissue default that is caused by insufficiently generated precursors.

Curiously, we show that MPCs were the only limb cells that showed robust BMP-dependent pSMAD expression at early limb bud stages, implying a high dependency of MPCs on BMP signaling. However, we neither explored the source of BMPs, nor which ligands of the BMP family signal to limb MPCs. In previous work, early migrating MPCs were found surrounded by BMP2/4/7-expressing cells at limb margins and ectopically applied BMP altered the positioning of premuscle masses in chick embryos (Amthor et al., 1998). Similar expression of BMPs in limb margins was also observed in mouse embryos (Michos et al., 2004). It remains to be determined whether long-range BMP signaling from limb margins could regulate MPCs. Alternative sources, including expression by MPCs themselves, must be considered. Of note, triple knockout of BMP2/4/7 in the apical ectodermal ridge caused polydactyly and does not affect limb outgrowth, whereas overexpression of the BMP antagonist gremlin in entire limb mesenchyme prevented limb outgrowth altogether (Choi et al., 2012; Norrie et al., 2014). However, muscle development has not been analyzed in these mutants.

The majority of MPCs is derived from migratory and *Pax3*-dependent MPCs of somite origin. However, recent work demonstrated a dual origin of MPCs in the developing limb: a small population of MCT cells is integrated into myotubes at muscle tips close to tendons in chicken and mouse muscles (Esteves de

Lima et al., 2021; Yaseen et al., 2021), a process being promoted by BMP signaling (Esteves de Lima et al., 2021). BMP gain- and loss-of-function experiments in chicken embryos demonstrated that BMP signaling balances the fibroblast-myoblast conversion and consequently the muscle pattern (Esteves de Lima et al., 2021). Here, we show that BMP signaling also regulates the somite-derived *Pax3*-dependent MPC lineage in mouse limbs. Cell-autonomous inhibition of BMP signaling in somite-derived MPCs caused absence of entire muscles. Therefore, MCT depends on the presence of somite-derived MPCs and are lost secondarily when muscle fails to develop. Further, the generation of the somite-independent muscle lineage depends on the presence of somite-derived muscle.

We found that the patterning defect in *Lbx1<sup>Cre</sup>;RS6* limbs persisted from embryonic to fetal stages, showing that secondary myogenesis cannot compensate for embryonic muscle defects, and remaining muscles continue to grow despite persistent inhibition of BMP signaling.

We would like to emphasize that our results support the MCT prepattern model (see Fig. S9). We believe that mesenchymal cells that form future MCT are the source of cues, including BMPs, that inform MPCs of where to migrate and proliferate. MCT and MPCs could be mutually dependent on each other to establish the muscle pattern. Indeed, a defined MCT pattern resembling a muscle pattern failed to develop in muscle-devoid limbs (Christ et al., 1977). Whereas tendons initially developed autonomously in lack of muscles; they degenerated secondarily (Christ et al., 1977; Schweitzer et al., 2010).

We here employed the overexpression of *huSMAD6* as a mean to test the cell-autonomous effect of abrogating BMP signaling. SMAD6 inhibits Smad signaling by the BMP type I receptors ALK-3/6 subgroup and only weakly inhibits TGF- $\beta$ /activin signaling via the BMP type I receptors ALK-1/2 subgroup, the latter being a preferential target of SMAD7 (Goto et al., 2007; Miyazawa and Miyazono, 2017). As SMAD6 is not a direct component of the BMP signaling cascade, further work is required to substantiate our results, such as performing specific BMP receptor knockout. In previous work, we showed that satellite cell-specific overexpression of *SMAD6* or knockout of *Alk3*, or overexpression of the BMP antagonist *Nog* in postnatal mice decreased proliferation of satellite cells, diminished their accretion during myofiber growth and retarded muscle growth, whereas overexpression of *SMAD6* exclusively in terminally differentiated myofibers did not affect satellite cell-dependent muscle growth (Stantzou et al., 2017). Together with herein presented results, this confirms that BMP signaling acts in a similar cell-autonomous manner in MPCs during prenatal and postnatal development.

In conclusion, our data suggest that BMP signaling controls embryonic limb MPCs to maintain PAX3-expressing precursor status, coordinates MPC migration, proliferation and myogenic lineage progression, thereby providing the cellular source that is required for building the correct muscle pattern. The expression of the Hox code in MPCs may indicate that positional identity is established before the splitting of pre-muscle masses into individual muscles. Future loss- and gain-of-function experiments are required to directly test the function of Hox gene expression in MPCs.

## MATERIALS AND METHODS

### Mouse lines used for embryo generation

We conducted all animal experiments according to national and European legislation as well as institutional guidelines for the care and use of laboratory animals as approved by the French government.

The following mouse lines have been previously described: *Lbx1<sup>Cre</sup>* mice (Sieber et al., 2007), *HSA-Cre* transgenic mice (Miniou et al., 1999),

*Rosa26<sup>LoxP-Stop-LoxP-huSMAD6-IRES-EGFP</sup>* mice (i.e. *RS6*) (Stantzou et al., 2017), and *Ai9* mice, which contain an insertion in the *Rosa26* locus of a strong and ubiquitous CAG promoter, followed by a floxed-Stop cassette-controlled *tdTomato* (Madisen et al., 2010).

*Lbx1<sup>Cre</sup>*, *HSA-Cre* and *RS6* mice were interbred to obtain *Lbx1<sup>Cre</sup>;RS6* and *HSA-Cre;RS6* embryos. *Lbx1<sup>Cre</sup>* and *Ai9* mice were interbred to obtain heterozygous *Lbx1<sup>Cre</sup>;Ai9* mice, which were crossed with *RS6* mice to obtain *Lbx1<sup>Cre</sup>;RS6/Ai9* embryos.

Genomic DNA isolated from ear clippings postnatally, or from yolk sacs or parts of the non-limb tissues prenatally, were genotyped. The PCR primers are described in Table S1.

### Embryonic and fetal forelimb collection and processing

Embryos and fetuses were collected in ice-cold phosphate-buffered saline (PBS) at different stages (plug date: E0.5). Embryos used for WISH experiments were fixed overnight in 4% paraformaldehyde (PFA) at 4°C, washed twice in PBS-T (PBS + 0.1% Tween-20, P9416, Sigma-Aldrich) and dehydrated using a methanol series of 50% methanol (15 min $\times$ 2) and 100% methanol (15 min), after which they were stored at -20°C for WISH.

For immunostaining, forelimbs from E10.5 and E11.5 embryos were dissected as pairs connected with the rostral (thoracic) body segment to preserve the structure of the forelimbs and forelimb-level somites. At the later stages, the forelimbs were individually dissected. The tissues were fixed at 4°C in either 1% PFA for 1 h (E10.5-E12.5) or in 4% PFA for 2 h (E14.5 and E18.5), washed thrice for 10 min and then dehydrated overnight at 4°C in either 15% sucrose (E10.5-E12.5) or 30% sucrose (E14.5 and E18.5). The forelimbs were embedded in Optimum Cutting Temperature compound (Qpath) in disposable plastic molds (Dutscher), frozen in liquid nitrogen and stored at -80°C for sectioning.

### RNA isolation and RT-qPCR

Total RNA from frozen E18.5 forelimb muscle tissue was extracted using TRIzol (Life Technologies Ambion) in combination with an RNeasy Mini kit (Qiagen). Traces of DNA in the RNA extract were removed with an RNase-Free DNase Set (Qiagen). The isolated RNA was quantified using a NanoVue Plus GE HealthCare spectrophotometer (Dutscher). Next, complementary DNA (cDNA) was synthesized using reverse transcriptase (SuperScript<sup>TM</sup> III First-Strand Synthesis SuperMix kit, Invitrogen). RT-qPCR was performed according to the SYBR Green protocol (Bio-Rad) in triplicate on a CFX96 Touch Real-Time detection system (Bio-Rad) using iTaq Universal SYBR Green Supermix (Bio-Rad) and primers for *huSMAD6* and the housekeeping gene *Gapdh* as described previously (Stantzou et al., 2017).

### WISH

WISH with digoxigenin-labeled probes was used for visualizing the expression of *Lbx1*, *Pax3* or *Myod*. WISH was performed as previously described (Murgai et al., 2018; Tajbakhsh et al., 1997).

### Immunofluorescence staining

Serial sections of frozen forelimbs on SuperFrost Plus adhesion slides (Thermo Fisher Scientific) were obtained at 10- $\mu$ m thickness using a cryostat (Leica, CM3050S) at -24°C. E10.5 and E11.5 forelimbs were longitudinally sectioned, which allowed 2D visualization of forelimb sections in the proximodistal and dorsoventral axes. E12.5, E14.5 and E18.5 forelimbs were sectioned in the transverse plane (except where stated otherwise), which allowed 2D visualization of forelimb sections in the dorsoventral and anteroposterior axes. The forelimb sections on the slides were directly used for immunofluorescence staining experiments or were stored at -80°C for future use.

Immunofluorescence staining was performed using the following protocols: (1) rehydration of slides in PBS for 5 min; (2) permeabilization with 0.1% (E10.5-E12.5) or 0.5% (E14.5 and E18.5) Triton X-100 (Sigma-Aldrich) (in the case of nuclear protein staining, e.g. PAX3, PAX7, MYOD, MYOG, pSMAD1/5/9, HOXA11, KI67, Caspase-3) or with methanol (for non-nuclear proteins, e.g. MHC, laminin alpha 2, DsRed, collagen 12) at -20°C; (3) three 5-min washes in PBS; (4) antigen retrieval by 20-min

immersion of the slides in boiled 10 mM citric acid solution kept at 60°C in a water bath; the slides were cooled at room temperature in the citric acid solution, and three PBS washes were performed (only for E14.5 and E18.5 nuclear staining); (5) up to 1.5-h blocking with 10% normal goat serum (Abcam); (6) overnight incubation with primary antibodies (dilutions prepared in blocking solution, Table S2) at 4°C; (7) three 5-min washes in PBS; (8) up to 1.5-h incubation with secondary antibodies (dilutions prepared in blocking solution, Table S3); (9) three 5-min washes in PBS; (10) incubation with DAPI for nuclear staining (10 min; dilution 1:5000); (11) washing in PBS for 5 min; (12) coverslip mounting with Fluoromount-G (Southern Biotech). Tables S2 and S3 detail the primary and secondary antibodies used in this study.

### Imaging

Embryos were dissected and whole limbs in the unfixed state were immediately imaged for native EGFP and tdTomato fluorescence using a stereomicroscope (SteREO Lumar.V12, Zeiss). Native EGFP and tdTomato fluorescence was subsequently imaged on fresh unfixed cryosections, and fluorescence immunohistochemistry was captured under 20×, 40× or 63× objective using a fluorescence microscope (Zeiss Axio Imager) with an Orkan camera (Hamamatsu). Images were acquired using AxioVision software. Mosaic images of immunostained whole limbs were obtained after stitching together multiple individual images captured with a 20× objective of all the different regions in the whole limb for all fluorescence channels of interest. Masson's trichrome staining images were acquired using a digital slide scanner (Leica) and analyzed with ImageScope software. Images were exported and saved as TIFF files for further analyses or for illustration in the figures.

### Morphometric studies

The captured fluorescent images were analyzed by applying morphometric studies using ImageJ (Schneider et al., 2012). The populations of cell and nuclear markers (PAX3, MYOD, PAX7, MYOG, KI67, HOXA11, DAPI) were quantified on immunostained cryosections as detailed above by superimposing fluorescence channels to visualize signal colocalization.

Proximodistal migration of PAX3-expressing MPCs in E10.5 forelimbs was quantified by dividing the forelimb into ten equally sized proximodistal zones and counting the PAX3<sup>+</sup> cells in each zone. Myofibers on the transverse sections of E14.5 forelimb zeugopods were quantified following co-immunostaining against laminin alpha 2 and MHC. Total muscle cross-sectional area (CSA) was determined as the sum of the CSA of all individual zeugopod muscles.

Morphometric studies at E10.5, E11.5 and E12.5 were conducted on three consecutive sections of each forelimb, and  $n=5$  forelimbs were analyzed for each genotype, except where stated otherwise. Morphometric studies at E14.5 were conducted on one transverse section through the proximal region of forelimb zeugopods, assuring measurements at the maximal size of the zeugopod muscle.

### scRNA-seq analysis of whole limb cells

The scRNA-seq protocol for E12.5 mouse whole limb cells is described by Rouco et al. (2021); that for chicken whole limb cells is described by Esteves de Lima et al. (2021). Briefly, scRNA-seq datasets were generated from whole forelimbs from two different E4 embryos and three different E6 embryos using a 10x Chromium Chip (10x Genomics) followed by sequencing with a High Output Flow Cell using an Illumina Nextseq 500 and by sequence analysis with Cell Ranger Single Cell Software Suite 3.0.2 (10x Genomics). Only mononucleated muscle cells were included in the datasets, as plurinucleated myotubes were excluded by the single-cell isolation protocol. Downstream clustering analysis of scRNA-seq data was performed using the Seurat package (v3.0) (Stuart et al., 2019) under R ('The R Project for Statistical Computing', v3.6.1) (Macosko et al., 2015). We then extracted the clusters identified as muscle clusters by the differential expression of the classical myogenic markers (*PAX7*, *MYOD*, *MYOG*) and performed the remaining analysis on these muscle clusters only. Gene expression was defined by 'gene log-normalized count >0'. The scRNA-seq datasets were analyzed using Seurat tools: FeaturePlot and Violin plots. Custom feature plots highlighting gene co-expression were generated using the R package ggplot2 v3.3.3 (Wickham,

2016). Population intersection plots were generated with the R package UpSetR v1.4.0 (Conway et al., 2017).

Within the muscle clusters, cells were grouped according to two identities, i.e. whether or not they expressed *HOXA* (*HOXA*<sup>+</sup> and *HOXA*<sup>-</sup>, respectively). The *HOXA*<sup>+</sup> identity was defined by the expression (i.e. gene log-normalized count >0) in a cell of at least one of the seven *HOXA* genes found in the muscle clusters (*HOXA4*, *HOXA5*, *HOXA6*, *HOXA7*, *HOXA9*, *HOXA10*, *HOXA11*). *HOXA*<sup>-</sup> identity was conferred to cells that expressed none of the seven *HOXA* genes. A BMP score was calculated using the AddModuleScore function for the well-characterized BMP transcriptional read-out genes *ID1*, *ID2* and *ID3*. Response to BMP signaling was then compared between these two identities using the Seurat tool Violin plots and the ggplot2 tool boxplots.

Both chicken and mouse scRNA-seq datasets used are deposited in the National Center for Biotechnology Information Gene Expression Omnibus database (<https://www.ncbi.nlm.nih.gov/geo/>), respectively under accession numbers GSE166981 and GSE168633.

### Statistical analyses

Numerical data are presented as the mean±s.d. The probability for statistical differences between experimental and control groups was determined by calculating the exact *P*-value using the non-parametric two-tailed Mann-Whitney *U*-test. GraphPad Prism Software version 7.00 for Windows ([www.graphpad.com](http://www.graphpad.com)) was used for all statistical analyses and graphs.

### Acknowledgements

We thank Prof. Dr Carmen Birchmeier (Developmental Biology and Signal Transduction Group, Max Delbrück Center for Molecular Medicine, Berlin, Germany) for providing the *Lbx1*<sup>Cre</sup> mice. Some of the text and figures in this paper formed part of Dr Hasan Asfour's PhD thesis in the department 'UFR Simone Veil – Santé' and in the unit 'UVSQ, Inserm, END-ICAP', at Paris-Saclay University, France, in 2021. We thank the animal and imaging facility of the UFR Simone Veil - Santé.

### Competing interests

The authors declare no competing or financial interests.

### Author contributions

Conceptualization: H. Asfour, K.P., F.R., G.A., S. Stricker, D.D., A.S., H. Amthor; Methodology: H. Asfour, E.H., R.R., F.Z., S.H., S. Swist, T.B., G.A., D.D., A.S., H. Amthor; Validation: H. Asfour, E.H., G.A., D.D., A.S., H. Amthor; Formal analysis: H. Asfour, E.H., G.A., D.D., A.S., H. Amthor; Investigation: H. Asfour, E.H., R.R., F.Z., S.H., G.A., D.D., A.S., H. Amthor; Resources: H. Asfour, E.H., R.R., S. Swist, T.B., F.R., G.A., D.D., A.S., H. Amthor; Writing - original draft: H. Asfour, A.S., H. Amthor; Writing - review & editing: H. Asfour, E.H., R.R., F.Z., S.H., S. Swist, T.B., K.P., F.R., G.A., S. Stricker, D.D., A.S., H. Amthor; Visualization: H. Asfour, R.R., A.S., H. Amthor; Supervision: F.R., G.A., D.D., A.S., H. Amthor; Project administration: H. Asfour, A.S., H. Amthor; Funding acquisition: H. Asfour, F.R., G.A., H. Amthor.

### Funding

Financial support was provided by: the Association Française contre les Myopathies (project funding number 20313 to H. Amthor, PhD funding number 21357 to H. Asfour, TRANSLAMUSCLE funding number 19507 to F.R., MyoConnect funding number 22234 to D.D.); the French state through the Agence Nationale de la Recherche (BMP-Myomass ANR-12-BSV1-0038-04 and BMP-Myostem ANR-16-CE14-0002-01 to H. Amthor, LimbCT ANR-20-CE13-0020-01 to D.D. and Labex REVIVE ANR-10-LABX-73 to F.R.); the Deutsch-Französische Hochschule (as part of the MyoGrad International Graduate School for Myology, CDFA-06-11, to H. Amthor); and the Schweizerischer Nationalfonds zur Förderung der Wissenschaftlichen Forschung (grant PP00P3\_176802 to G.A.).

### Data availability

All relevant data can be found within the article and its supplementary information.

### Peer review history

The peer review history is available online at <https://journals.biologists.com/dev/lookup/doi/10.1242/dev.201504.reviewer-comments.pdf>.

### References

Amthor, H., Christ, B., Weil, M. and Patel, K. (1998). The importance of timing differentiation during limb muscle development. *Curr. Biol.* **8**, 642-652. doi:10.1016/S0960-9822(98)70251-9

- Blagden, C. S. and Hughes, S. M. (1999). Extrinsic influences on limb muscle organisation. *Cell Tissue Res.* **296**, 141-150. doi:10.1007/s004410051275
- Bober, E., Franz, T., Arnold, H. H., Gruss, P. and Tremblay, P. (1994). Pax-3 is required for the development of limb muscles: a possible role for the migration of dermomyotomal muscle progenitor cells. *Development* **120**, 603-612. doi:10.1242/dev.120.3.603
- Brohmann, H., Jagla, K. and Birchmeier, C. (2000). The role of Lbx1 in migration of muscle precursor cells. *Development* **127**, 437-445. doi:10.1242/dev.127.2.437
- Choi, K.-S., Lee, C., Maatouk, D. M. and Harfe, B. D. (2012). Bmp2, Bmp4 and Bmp7 are co-required in the mouse AER for normal digit patterning but not limb outgrowth. *PLoS ONE* **7**, e37826. doi:10.1371/journal.pone.0037826
- Christ, B. and Brand-Saberi, B. (2002). Limb muscle development. *Int. J. Dev. Biol.* **46**, 905-914.
- Christ, B., Jacob, H. J. and Jacob, M. (1977). [Experimental findings on muscle development in the limbs of the chick embryo]. *Verh. Anat. Ges.* **71**, 1231-1237.
- Colasanto, M. P., Eyal, S., Mohassel, P., Bamshad, M., Bonnemann, C. G., Zelzer, E., Moon, A. M. and Kardon, G. (2016). Development of a subset of forelimb muscles and their attachment sites requires the ulnar-mammary syndrome gene *Tbx3*. *Dis. Model. Mech.* **143**, e1.1. doi:10.1242/dev.147645
- Conway, J. R., Lex, A. and Gehlenborg, N. (2017). UpSetR: an R package for the visualization of intersecting sets and their properties. *Bioinformatics* **33**, 2938-2940. doi:10.1093/bioinformatics/btx364
- Esteves De Lima, J., Blavet, C., Bonnin, M.-A., Hirsinger, E., Comai, G., Yvernogeu, L., Delfini, M.-C., Bellenger, L., Mella, S., Nassari, S. et al. (2021). Unexpected contribution of fibroblasts to muscle lineage as a mechanism for limb muscle patterning. *Nat. Commun.* **12**, 3851. doi:10.1038/s41467-021-24157-x
- Fromental-Ramain, C., Warot, X., Messadecq, N., Lemeur, M., Dollé, P. and Chambon, P. (1996). Hoxa-13 and Hoxd-13 play a crucial role in the patterning of the limb autopod. *Development* **122**, 2997-3011. doi:10.1242/dev.122.10.2997
- Goto, K., Kamiya, Y., Imamura, T., Miyazono, K. and Miyazawa, K. (2007). Selective inhibitory effects of Smad6 on bone morphogenetic protein type I receptors. *J. Biol. Chem.* **282**, 20603-20611. doi:10.1074/jbc.M702100200
- Grim, M. and Wachtler, F. (1991). Muscle morphogenesis in the absence of myogenic cells. *Anat. Embryol.* **193**, 67-70. doi:10.1007/BF00185836
- Hashimoto, K., Yokouchi, Y., Yamamoto, M. and Kuroiwa, A. (1999). Distinct signaling molecules control Hoxa-11 and Hoxa-13 expression in the muscle precursor and mesenchyme of the chick limb bud. *Development* **126**, 2771-2783. doi:10.1242/dev.126.12.2771
- Hasson, P., Delaurier, A., Bennett, M., Grigorieva, E., Naiche, L. A., Papaioannou, V. E., Mohun, T. J. and Logan, M. P. O. (2010). *Tbx4* and *Tbx5* acting in connective tissue are required for limb muscle and tendon patterning. *Dev. Cell* **18**, 148-156. doi:10.1016/j.devcel.2009.11.013
- Hata, A., Lagna, G., Massagué, J. and Hemmati-Brivanlou, A. (1998). Smad6 inhibits BMP/Smad1 signaling by specifically competing with the Smad4 tumor suppressor. *Genes Dev.* **12**, 186-197. doi:10.1101/gad.12.2.186
- Huang, A. H. (2017). Coordinated development of the limb musculoskeletal system: tendon and muscle patterning and integration with the skeleton. *Dev. Biol.* **429**, 420-428. doi:10.1016/j.ydbio.2017.03.028
- Huang, A. H., Riordan, T. J., Pryce, B., Weibel, J. L., Watson, S. S., Long, F., Lefebvre, V., Harfe, B. D., Stadler, H. S., Akiyama, H. et al. (2015). Musculoskeletal integration at the wrist underlies the modular development of limb tendons. *Development* **142**, 2431-2441. doi:10.1242/dev.122374
- Kardon, G., Campbell, J. K. and Tabin, C. J. (2002). Local extrinsic signals determine muscle and endothelial cell fate and patterning in the vertebrate limb. *Dev. Cell* **3**, 533-545. doi:10.1016/S1534-5807(02)00291-5
- Kardon, G., Harfe, B. D. and Tabin, C. J. (2003). A Tcf4-positive mesodermal population provides a prepattern for vertebrate limb muscle patterning. *Dev. Cell* **5**, 937-944. doi:10.1016/S1534-5807(03)00360-5
- Lagha, M., Kormish, J. D., Rocancourt, D., Manceau, M., Epstein, J. A., Zaret, K. S., Relaix, F. and Buckingham, M. E. (2008). Pax3 regulation of FGF signaling affects the progression of embryonic progenitor cells into the myogenic program. *Genes Dev.* **22**, 1828-1837. doi:10.1101/gad.477908
- Lepper, C. and Fan, C.-M. (2010). Inducible lineage tracing of Pax7-descendant cells reveals embryonic origin of adult satellite cells. *Genesis* **48**, 424-436. doi:10.1002/dvg.20630
- Macosko, E. Z., Basu, A., Satija, R., Nemes, J., Shekhar, K., Goldman, M., Tirosh, I., Bialas, A. R., Kamitaki, N., Martersteck, E. M. et al. (2015). Highly parallel genome-wide expression profiling of individual cells using nanoliter droplets. *Cell* **161**, 1202-1214. doi:10.1016/j.cell.2015.05.002
- Madisen, L., Zwingman, T. A., Sun, S. M., Oh, S. W., Zariwala, H. A., Gu, H., Ng, L. L., Palmiter, R. D., Hawrylycz, M. J., Jones, A. R. et al. (2010). A robust and high-throughput Cre reporting and characterization system for the whole mouse brain. *Nat. Neurosci.* **13**, 133-140. doi:10.1038/nn.2467
- Michos, O., Panman, L., Vintersten, K., Beier, K., Zeller, R. and Zuniga, A. (2004). Gremlin-mediated BMP antagonism induces the epithelial-mesenchymal feedback signaling controlling metanephric kidney and limb organogenesis. *Development* **131**, 3401-3410. doi:10.1242/dev.01251
- Minou, P., Tiziano, D., Frugier, T., Roblot, N., Le Meur, M. and Melki, J. (1999). Gene targeting restricted to mouse striated muscle lineage. *Nucleic Acids Res.* **27**, e27. doi:10.1093/nar/27.19.e27
- Miyazawa, K. and Miyazono, K. (2017). Regulation of TGF- $\beta$  family signaling by inhibitory Smads. *Cold Spring Harb. Perspect. Biol.* **9**, a022095. doi:10.1101/cshperspect.a022095
- Murakami, G., Watabe, T., Takaoka, K., Miyazono, K. and Imamura, T. (2003). Cooperative inhibition of bone morphogenetic protein signaling by Smurf1 and inhibitory Smads. *Mol. Biol. Cell* **14**, 2809-2817. doi:10.1091/mbc.e02-07-0441
- Murgai, A., Altmeyer, S., Wiegand, S., Tylzanowski, P. and Stricker, S. (2018). Cooperation of BMP and IHH signaling in interdigital cell fate determination. *PLoS ONE* **13**, e0197535. doi:10.1371/journal.pone.0197535
- Nohe, A., Hassel, S., Ehrlich, M., Neubauer, F., Sebald, W., Henis, Y. I. and Knaus, P. (2002). The mode of bone morphogenetic protein (BMP) receptor oligomerization determines different BMP-2 signaling pathways. *J. Biol. Chem.* **277**, 5330-5338. doi:10.1074/jbc.M102750200
- Nohe, A., Keating, E., Knaus, P. and Petersen, N. O. (2004). Signal transduction of bone morphogenetic protein receptors. *Cell. Signal.* **16**, 291-299. doi:10.1016/j.cellsig.2003.08.011
- Norrie, J. L., Lewandowski, J. P., Bouldin, C. M., Amarnath, S., Li, Q., Vokes, M. S., Ehrlich, L. I. R., Harfe, B. D. and Vokes, S. A. (2014). Dynamics of BMP signaling in limb bud mesenchyme and polydactyly. *Dev. Biol.* **393**, 270-281. doi:10.1016/j.ydbio.2014.07.003
- Pownall, M. E., Gustafsson, M. K. and Emerson, C. P. (2002). Myogenic regulatory factors and the specification of muscle progenitors in vertebrate embryos. *Annu. Rev. Cell Dev. Biol.* **18**, 747-783. doi:10.1146/annurev.cellbio.18.012502.105758
- Relaix, F., Rocancourt, D., Mansouri, A. and Buckingham, M. (2005). A Pax3/Pax7-dependent population of skeletal muscle progenitor cells. *Nature* **435**, 948-953. doi:10.1038/nature03594
- Rouco, R., Bompadre, O., Rauseo, A., Fazio, O., Thorel, F., Peraldi, R. and Andrey, G. (2021). Cell-specific alterations in Ptx1 regulatory landscape activation caused by the loss of a single enhancer. *Nat. Commun.* **12**, 7235. doi:10.1038/s41467-021-27492-1
- Schneider, C. A., Rasband, W. S. and Eliceiri, K. W. (2012). NIH Image to ImageJ: 25 years of image analysis. *Nat. Methods* **9**, 671-675. doi:10.1038/nmeth.2089
- Schweitzer, R., Zelzer, E. and Volk, T. (2010). Connecting muscles to tendons: tendons and musculoskeletal development in flies and vertebrates. *Development* **137**, 2807-2817. doi:10.1242/dev.047498
- Shin, J., Watanabe, S., Hoelper, S., Krüger, M., Kostin, S., Pöling, J., Kubin, T. and Braun, T. (2016). BRAF activates PAX3 to control muscle precursor cell migration during forelimb muscle development. *eLife* **5**, e18351. doi:10.7554/eLife.18351
- Sieber, M. A., Storm, R., Martinez-De-La-Torre, M., Müller, T., Wende, H., Reuter, K., Vasyutina, E. and Birchmeier, C. (2007). Lbx1 acts as a selector gene in the fate determination of somatosensory and viscerosensory relay neurons in the hindbrain. *J. Neurosci.* **27**, 4902-4909. doi:10.1523/JNEUROSCI.0717-07.2007
- Stantzu, A., Schirwis, E., Swist, S., Alonso-Martin, S., Polydorou, I., Zarrouki, F., Mouisel, E., Beley, C., Julien, A., Le Grand, F. et al. (2017). BMP signaling regulates satellite cell-dependent postnatal muscle growth. *Development* **144**, 2737-2747. doi:10.1242/dev.144089
- Stuart, T., Butler, A., Hoffman, P., Hafemeister, C., Papalexi, E., Mauck, W. M., Hao, Y., Stoeckius, M., Smibert, P. and Satija, R. (2019). Comprehensive integration of single-cell data. *Cell* **177**, 1888-1902.e21. doi:10.1016/j.cell.2019.05.031
- Sundin, O. H., Busse, H. G., Rogers, M. B., Gudas, L. J. and Eichele, G. (1990). Region-specific expression in early chick and mouse embryos of Ghox-lab and Hox 1.6, vertebrate homeobox-containing genes related to Drosophila labial. *Development* **108**, 47-58. doi:10.1242/dev.108.1.47
- Swinehart, I. T., Schlientz, A. J., Quintanilla, C. A., Mortlock, D. P. and Wellik, D. M. (2013). Hox11 genes are required for regional patterning and integration of muscle, tendon and bone. *Development* **140**, 4574-4582. doi:10.1242/dev.096693
- Tajbakhsh, S., Rocancourt, D., Cossu, G. and Buckingham, M. (1997). Redefining the genetic hierarchies controlling skeletal myogenesis: Pax-3 and Myf-5 act upstream of MyoD. *Cell* **89**, 127-138. doi:10.1016/S0092-8674(00)80189-0
- Tozer, S., Bonnin, M.-A., Relaix, F., Di Savino, S., García-Villalba, P., Coumilleau, P. and Duprez, D. (2007). Involvement of vessels and PDGFB in muscle splitting during chick limb development. *Development* **134**, 2579-2591. doi:10.1242/dev.02867
- Vallecillo-García, P., Orgeur, M., Vom Hofe-Schneider, S., Stumm, J., Kappert, V., Ibrahim, D. M., Börho, S. T., Hayashi, S., Relaix, F., Hildebrandt, K. et al. (2017). Odd skipped-related 1 identifies a population of embryonic fibro-adipogenic progenitors regulating myogenesis during limb development. *Nat. Commun.* **8**, 1218. doi:10.1038/s41467-017-01120-3
- Vasyutina, E., Stebler, J., Brand-Saberi, B., Schulz, S., Raz, E. and Birchmeier, C. (2005). CXCR4 and Gab1 cooperate to control the development of migrating muscle progenitor cells. *Genes Dev.* **19**, 2187-2198. doi:10.1101/gad.346205

- Wang, H., Noulet, F., Edom-Vovard, F., Le Grand, F. and Duprez, D.** (2010). Bmp signaling at the tips of skeletal muscles regulates the number of fetal muscle progenitors and satellite cells during development. *Dev. Cell* **18**, 643-654. doi:10.1016/j.devcel.2010.02.008
- Wickham, H.** (2016). *ggplot2: Elegant Graphics for Data Analysis*, 2nd edn. 2016 édn. New York, NY: Springer.
- Wood, W. M., Etemad, S., Yamamoto, M. and Goldhamer, D. J.** (2013). MyoD-expressing progenitors are essential for skeletal myogenesis and satellite cell development. *Dev. Biol.* **384**, 114-127. doi:10.1016/j.ydbio.2013.09.012
- Yakushiji-Kaminatsui, N., Lopez-Delisle, L., Bolt, C. C., Andrey, G., Beccari, L. and Duboule, D.** (2018). Similarities and differences in the regulation of HoxD genes during chick and mouse limb development. *PLoS Biol.* **16**, e3000004. doi:10.1371/journal.pbio.3000004
- Yamamoto, M. and Kuroiwa, A.** (2003). Hoxa-11 and Hoxa-13 are involved in repression of MyoD during limb muscle development. *Dev. Growth Differ.* **45**, 485-498. doi:10.1111/j.1440-169X.2003.00715.x
- Yamamoto, M., Gotoh, Y., Tamura, K., Tanaka, M., Kawakami, A., Ide, H. and Kuroiwa, A.** (1998). Coordinated expression of Hoxa-11 and Hoxa-13 during limb muscle patterning. *Development* **125**, 1325-1335. doi:10.1242/dev.125.7.1325
- Yaseen, W., Kraft-Sheleg, O., Zaffryar-Eilol, S., Melamed, S., Sun, C., Millay, D. P. and Hasson, P.** (2021). Fibroblast fusion to the muscle fiber regulates myotendinous junction formation. *Nat. Commun.* **12**, 3852. doi:10.1038/s41467-021-24159-9
- Zakany, J. and Duboule, D.** (2007). The role of Hox genes during vertebrate limb development. *Curr. Opin. Genet. Dev.* **17**, 359-366. doi:10.1016/j.gde.2007.05.011

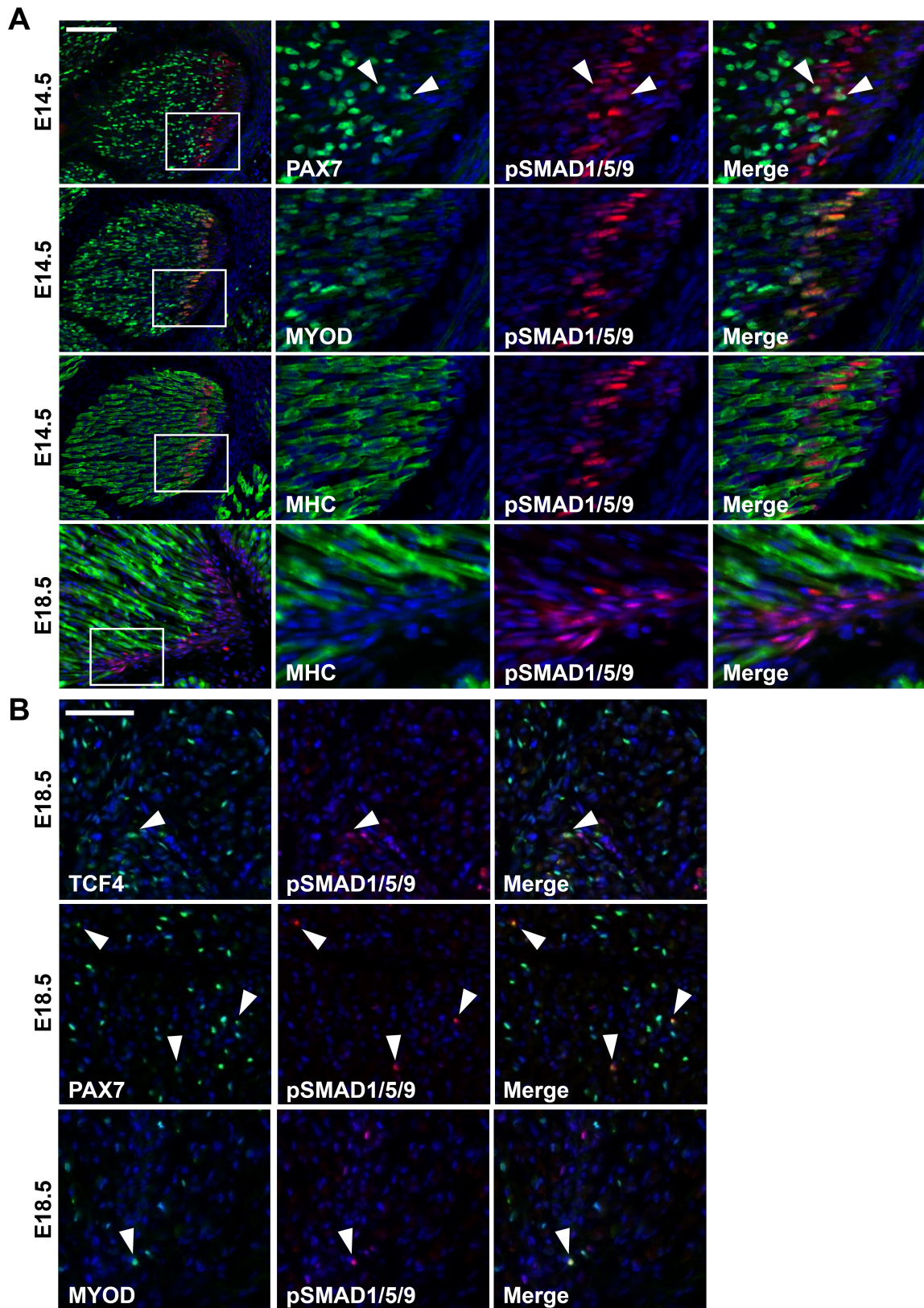


**Fig. S1. BMP signaling during embryonic and fetal myofiber formation. (A)** Left images show longitudinal sections through the *biceps brachii* muscle at E14.5 and E18.5 following co-immunostaining against pSMAD1/5/9 (red) with PAX7, MYOD or MHC (green). Nuclei are stained with DAPI (blue). Insets (white boxes) are shown at higher magnification on the right side of the respective *biceps brachii* muscle and depict individual and merged fluorescence channels. White arrowheads show the rare PAX7<sup>+</sup> cells at the fiber tips positive for pSMADs. *n* = 5 biological replicates for each immunostaining and developmental stage. Scale bar = 100  $\mu$ m. **(B)** Images depict immunofluorescence of pSMAD1/5/9 (red) together with TCF4, PAX7 or MYOD (green) at high magnification after co-immunostaining on transverse sections of forelimb zeugopod from E18.5 *RS6* control fetuses. Arrowheads indicate rare cells co-expressing pSMAD1/5/9 with TCF4 (top), PAX7 (middle) or MYOD (bottom). *n* = 5 biological replicates. Scale bar = 50  $\mu$ m.



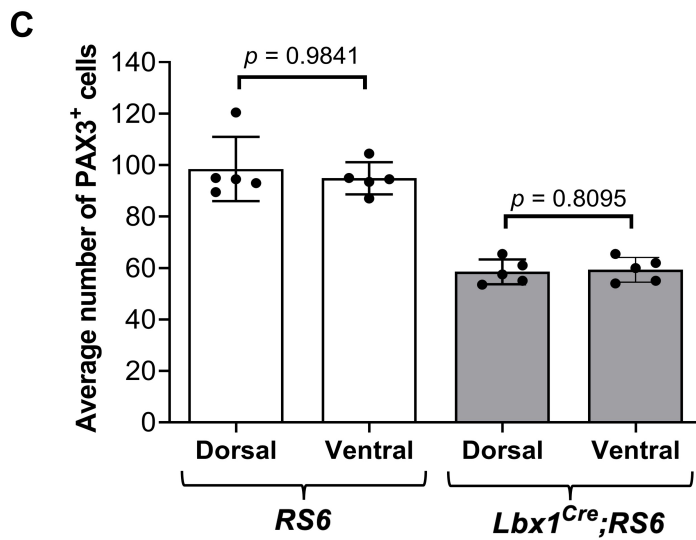
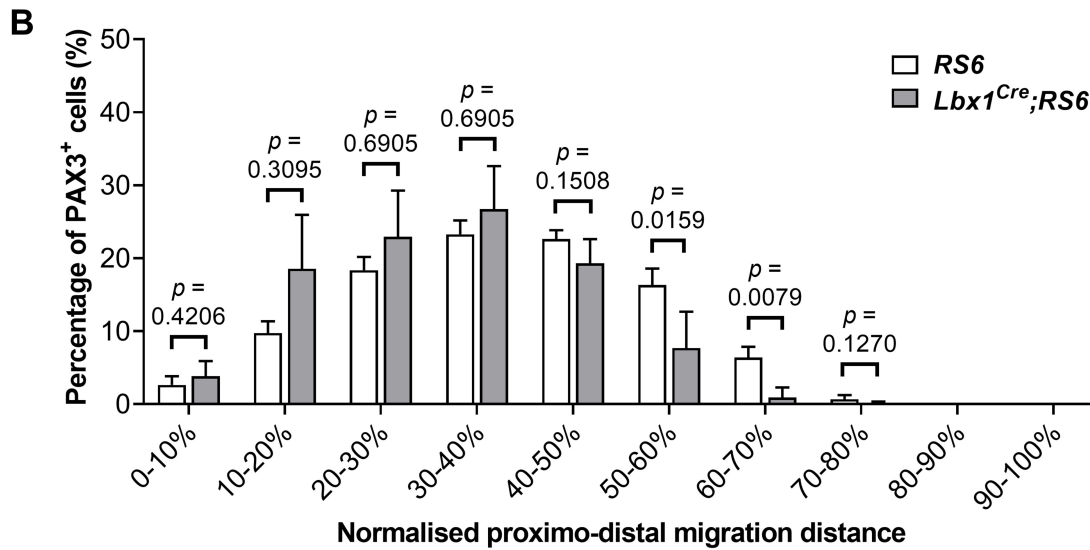
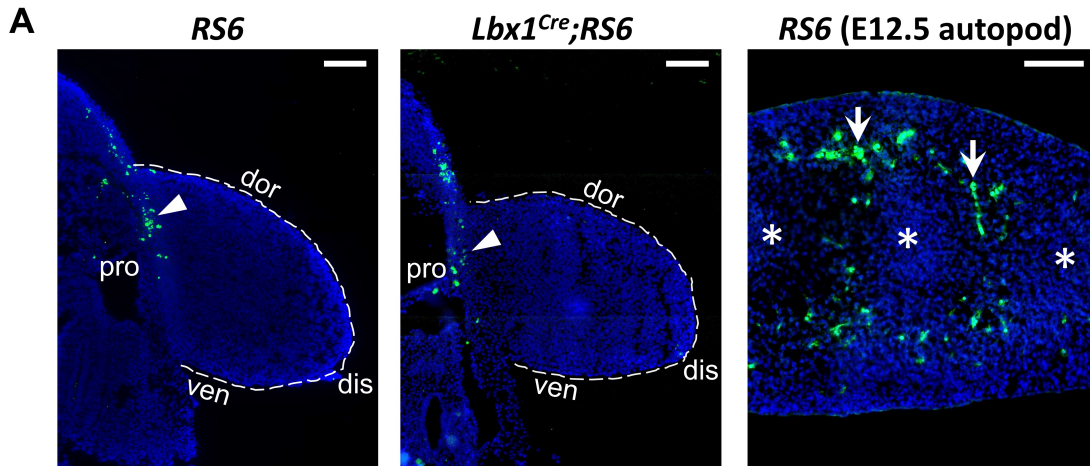


**Fig. S2. Effect of *SMAD6* overexpression on limb MPC number and distribution. (A)** Images depict immunofluorescence staining of cleaved Caspase-3 (green) following immunohistochemistry on longitudinal sections of E10.5 entire forelimbs of *RS6* control and *Lbx1<sup>Cre</sup>;RS6* embryos (left and middle images), and on a transverse section of a E12.5 autopod of a *RS6* control (right image). Nuclei are stained with DAPI (blue) (dor: dorsal; ven: ventral). Arrowheads mark cleaved Caspase-3<sup>+</sup> cells at the trunk level (left and middle images), arrows mark cleaved Caspase-3<sup>+</sup> cells in interdigital mesenchyme and asterisks mark mesenchymal cores of developing digits (right image). Scale bar = 100  $\mu$ m. **(B)** Histogram depicts the relative number of PAX3<sup>+</sup> MPCs based on their position along the proximodistal limb axis as depicted in Figure 4b. **(C)** Dot-plotted bar graph shows the number of PAX3<sup>+</sup> cells in the dorsal and ventral premuscle masses of forelimbs for both genotypes.  $n = 5$  biological replicates for each genotype. Each replicate represents the mean of three consecutive serial sections. Data are the mean  $\pm$  SD.

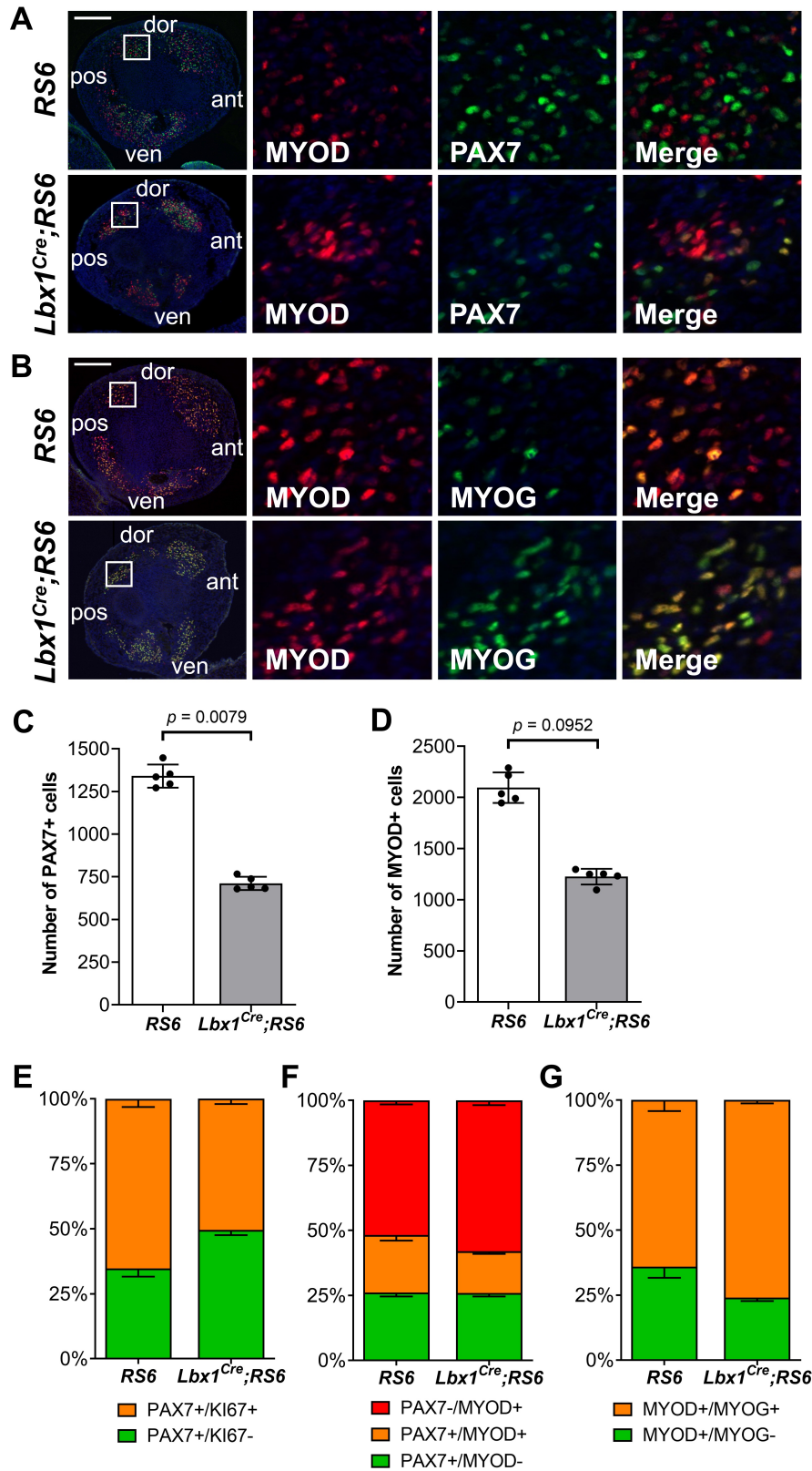


**Fig. S3. Effect of *SMAD6* overexpression on myogenic lineage progression in embryonic forelimb.** **(A and B)** Left images depict immunofluorescence staining of MYOD (red) in combination with PAX7 (green) **(A)**, or MYOG (green) **(B)** following co-immunohistochemistry on transverse sections of E12.5 forelimbs of *RS6* and *Lbx1<sup>Cre</sup>;RS6* embryos. Nuclei are stained with DAPI (blue). Insets (white solid lines) are shown at higher magnification on the right and depict individual and merged fluorescence channels. Scale bar = 200  $\mu$ m (ant: anterior; pos: posterior; dor: dorsal; ven: ventral). **(C and D)** Dot-plotted bar charts show the number of PAX7<sup>+</sup> and MYOD<sup>+</sup> cells. **(E)** Stacked bar graphs depict the percentages of PAX7<sup>+</sup>/KI67<sup>+</sup> cells (orange) ( $p = 0.0079$ ) and PAX7<sup>+</sup>/KI67<sup>-</sup> cells (green) ( $p = 0.0079$ ). **(F)** Stacked bar graph depicts the percentages of PAX7<sup>+</sup>/MYOD<sup>-</sup> cells (green) ( $p = 0.8413$ ), PAX7<sup>+</sup>/MYOD<sup>+</sup> cells (orange) ( $p = 0.0079$ ) and PAX7<sup>-</sup>/MYOD<sup>+</sup> cells (red) ( $p = 0.0079$ ). **(G)** Stacked bar graph depicts the percentages of MyoD<sup>+</sup>/MYOG<sup>-</sup> cells (green) ( $p = 0.0079$ ) and MYOD<sup>+</sup>/MYOG<sup>+</sup> cells (orange) ( $p = 0.0079$ ). MYOD<sup>-</sup>/MYOG<sup>+</sup> cells were not observed.  $n = 5$  biological replicates for each condition. Each replicate represents the mean of three consecutive serial sections. Data are the mean  $\pm$  SD.

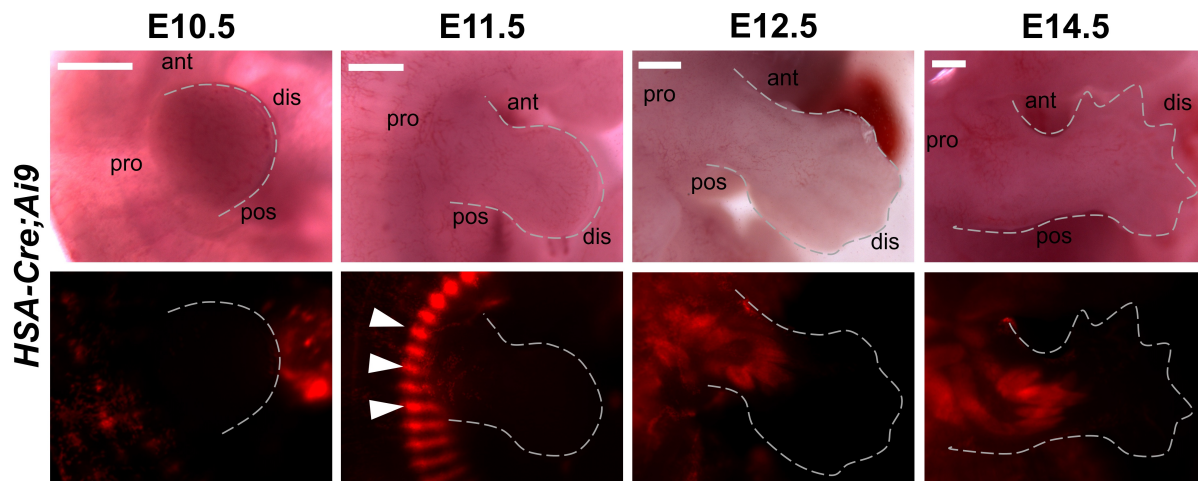


**Fig. S4. Spatiotemporal onset of HSA-Cre driven recombination.** Images show dorsal view of embryos at the forelimb level of E10.5–E14.5 *HSA-Cre;Ai9* embryos. Upper images show freshly dissected embryos using reflected light; lower images depict native tdTomato fluorescence (red). White arrowheads highlight tdTomato in somites at E11.5 (pro: proximal; dis: distal; ant: anterior; pos: posterior).  $n = 5$  biological replicates for each condition. Scale bars = 500  $\mu\text{m}$ .

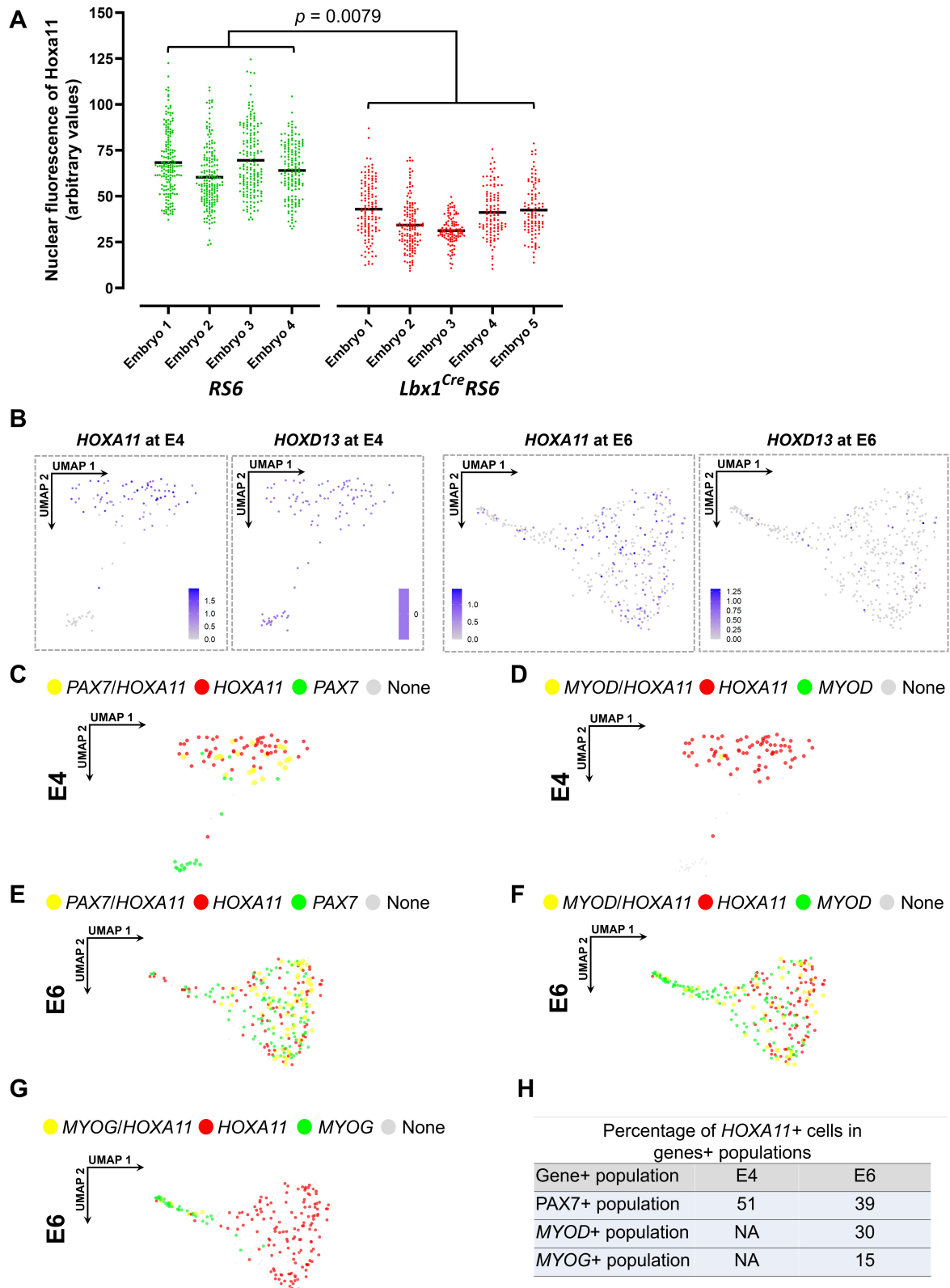


**Fig. S5. HOX gene expression in chicken MPCs. (A)** A ggplot2 dot-plot graph shows the quantified nuclear fluorescence (using arbitrary values) of HOXA11 protein in forelimb MPCs of *RS6* and *Lbx1<sup>Cre</sup>;RS6* genotypes at E10.5. Quantification was conducted on longitudinal sections of E10.5 forelimb buds co-stained for PAX3 and HOXA11.  $n = 4$  biological replicates for *RS6* and  $n = 5$  for *Lbx1<sup>Cre</sup>;RS6*. The  $p$ -value was calculated by comparing the means of both groups. **(B)** Uniform manifold approximation and projection (UMAP) of E4 and E6 chicken forelimb cells following scRNAseq depict the distribution of *HOXA11* and *HOXD13* expression in the cells of the muscle cluster. **(C-G)** Co-expression analysis of *HOXA11* gene and myogenic markers in chicken MPCs. UMAP depicts the co-expression of *HOXA11* with *PAX7* **(C, E)**, *MYOD* **(D, F)** and *MYOG* **(G)** or single-gene expression in the muscle cluster cells of chicken E4 forelimbs **(C, D)** and E6 forelimbs **(E, F, G)**. **(H)** Table summarizes the percentages of double expression cell populations shown in **(C-G)**.

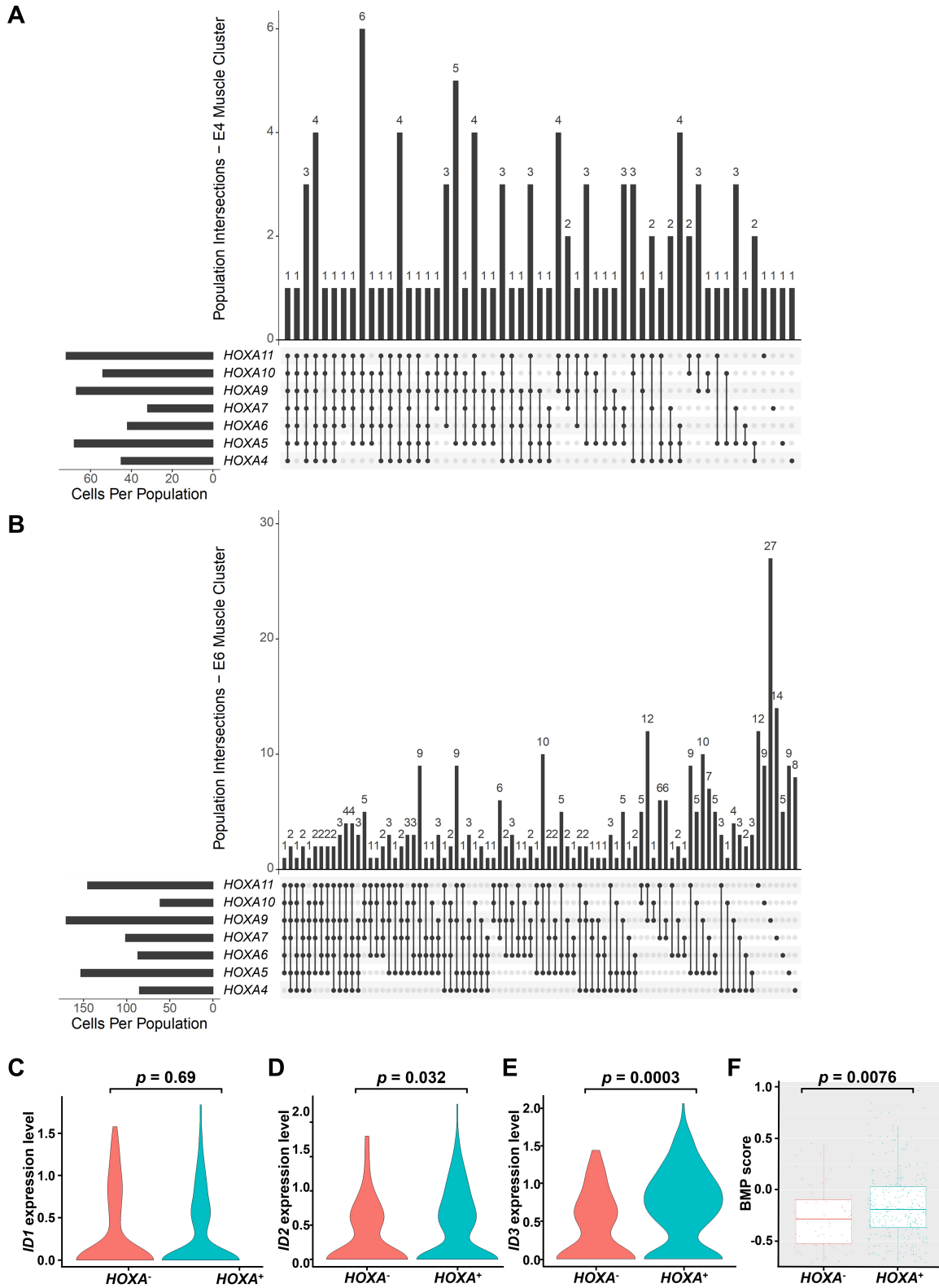




**Fig. S6. Analysis of *HOXA* gene expression and BMP transcriptional targets in chicken MPCs.** **(A-B)** Diagrams depict the muscle cluster cells expressing *HOXA* genes in E4 **(A)** and E6 chicken forelimbs **(B)**. The vertical bar plots represent the number of cells for the corresponding combination of *HOXA* genes, which is shown underneath the blot. The combinations for which there were no cells are not represented. The graphs are ordered by decreasing degree (i.e. the combination with the highest number of genes is on the left). The horizontal bar plots on the bottom left show the size of the population positive for the corresponding *HOX* gene. **(C-F)** Analysis of BMP transcriptional targets in muscle cluster cells of E6 chicken forelimbs. **(C, D, E)** Violin plots comparing the distribution of the expression levels of *ID1*, *ID2* and *ID3* between the *HOXA*<sup>-</sup> and *HOXA*<sup>+</sup> cell populations. The width of the violin plot indicates the number of cells that show the corresponding gene expression level. **(F)** Box plot comparing the BMP score (combined expression levels of *ID1*, *ID2* and *ID3*) between the *HOXA*<sup>-</sup> and *HOXA*<sup>+</sup> cell populations.

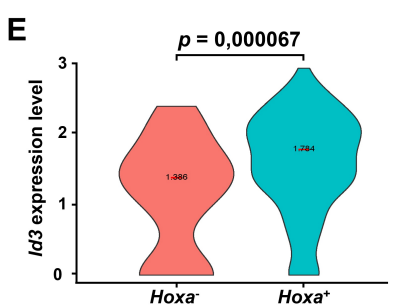
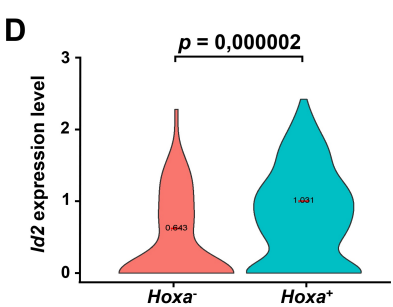
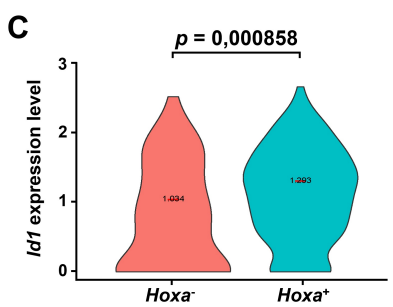
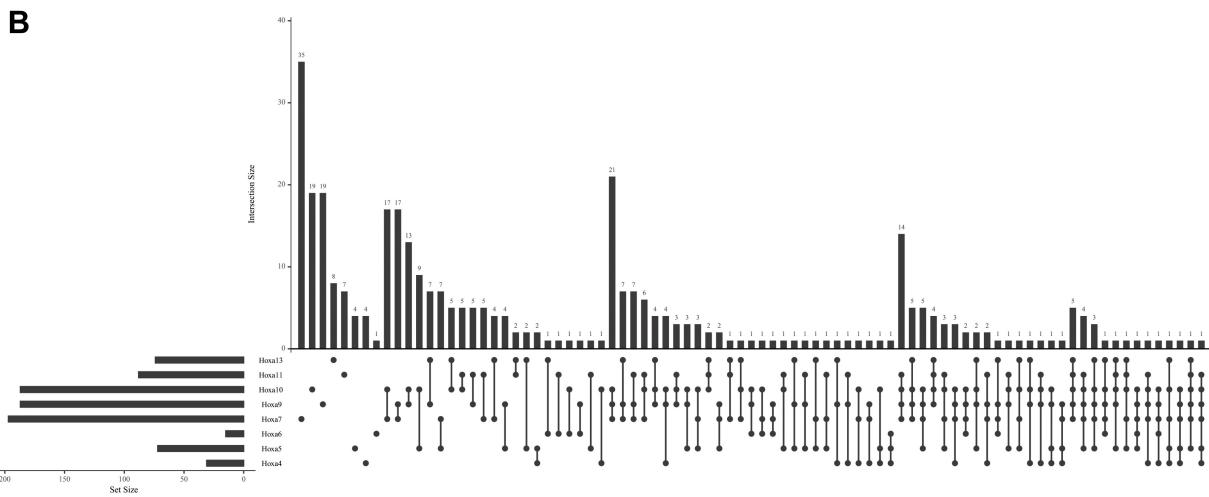
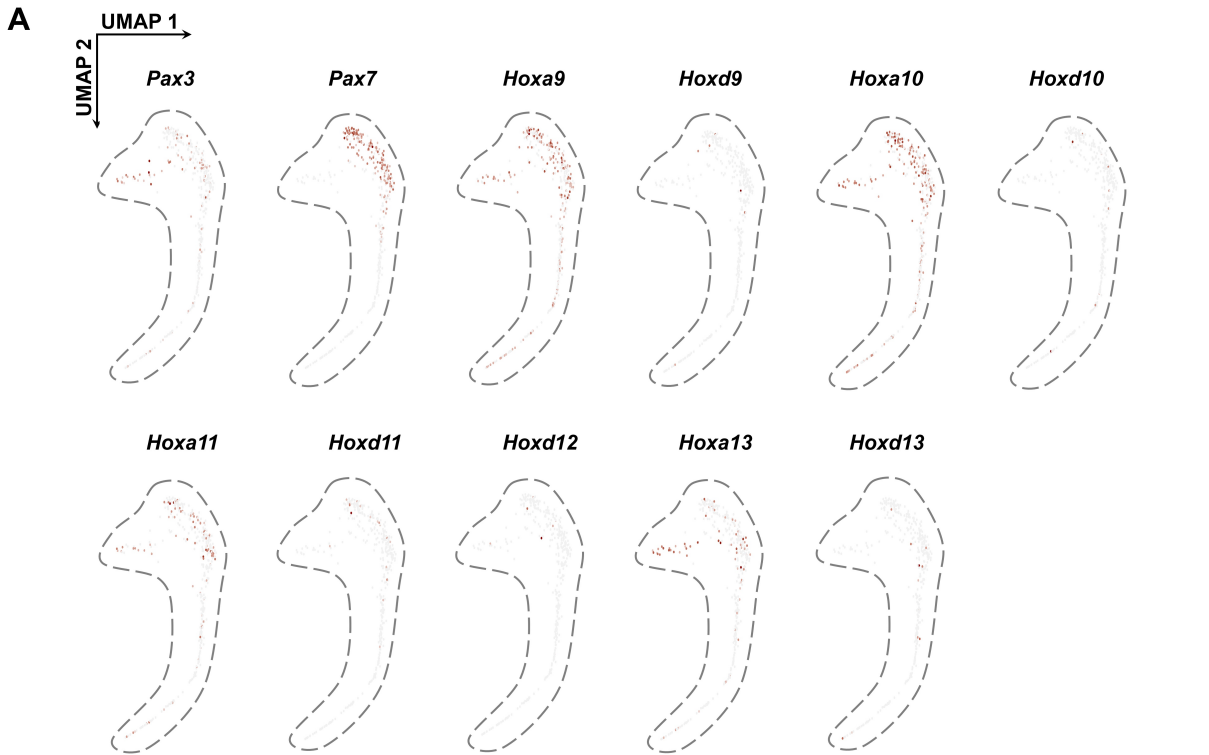


**Fig. S7. Analysis of *Hox* gene expression and BMP transcriptional targets in E12.5 mouse MPCs. (A)** UMAP of E12.5 mouse forelimb muscle cluster cells following scRNAseq. Expression distribution of selected marker genes across the muscle cluster. **(B)** Analysis of *Hoxa* genes expression. The vertical bar plots represent the number of cells for the corresponding combination of *Hoxa* genes, which is shown underneath the blot. The combinations for which there were no cells are not represented. The horizontal bar plots on the bottom left show the size of the population positive for the corresponding *Hox* gene. **(C-E)** Violin plots compare the distribution of the expression levels of *Id1*, *Id2* and *Id3* between the *Hoxa*<sup>-</sup> and *Hoxa*<sup>+</sup> cell populations. The width of the violin plot indicates the number of cells that show the corresponding gene expression level.

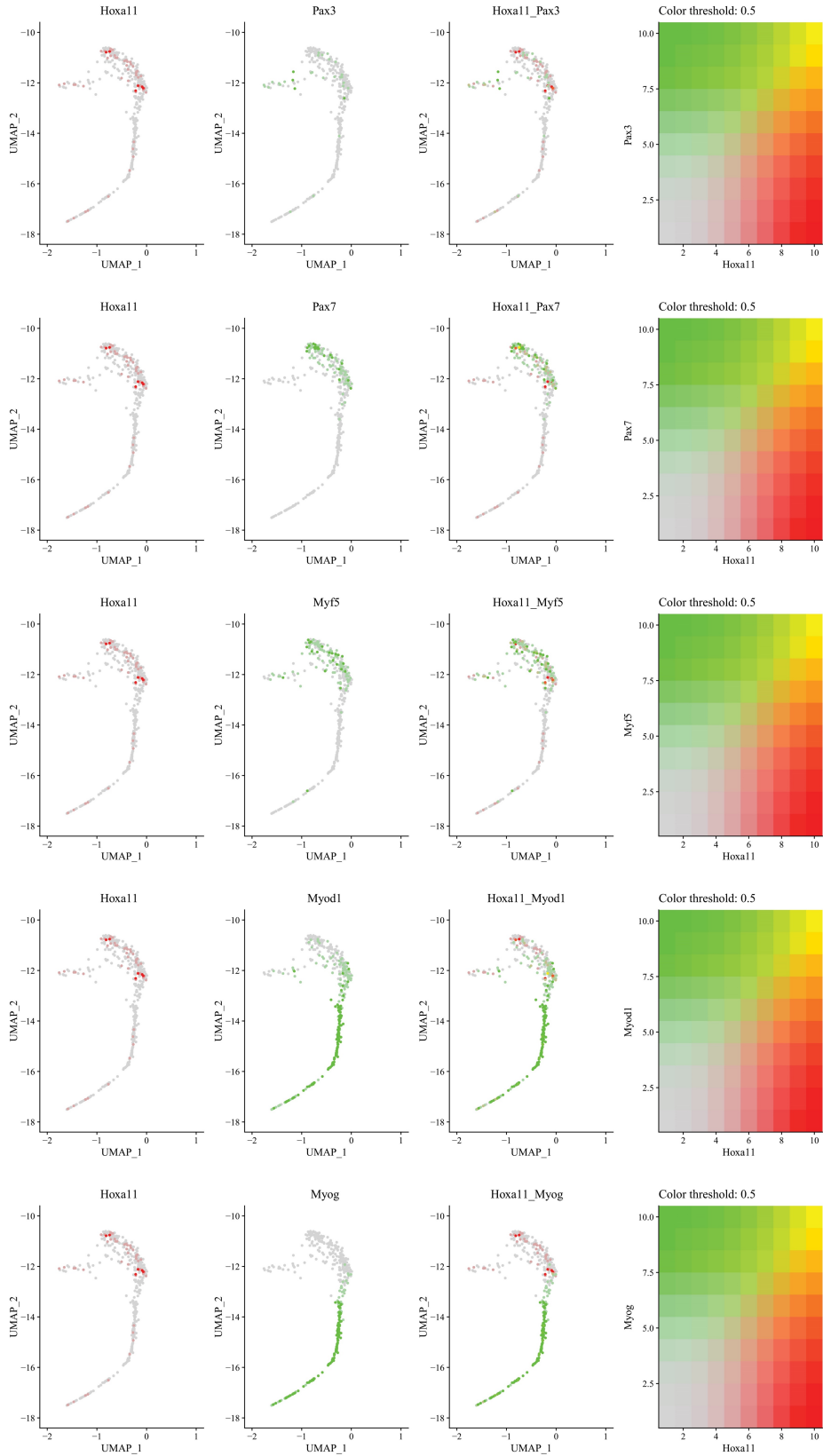


**Fig. S8. Co-expression analysis of *Hoxa11* gene and myogenic markers in mouse MPCs.** UMAP depicts single-gene expression or co-expression of *Hoxa11* with *Pax3*, *Pax7*, *Myf5*, *Myod* and *Myog* in the muscle cluster cells of E12.5 mouse forelimbs.

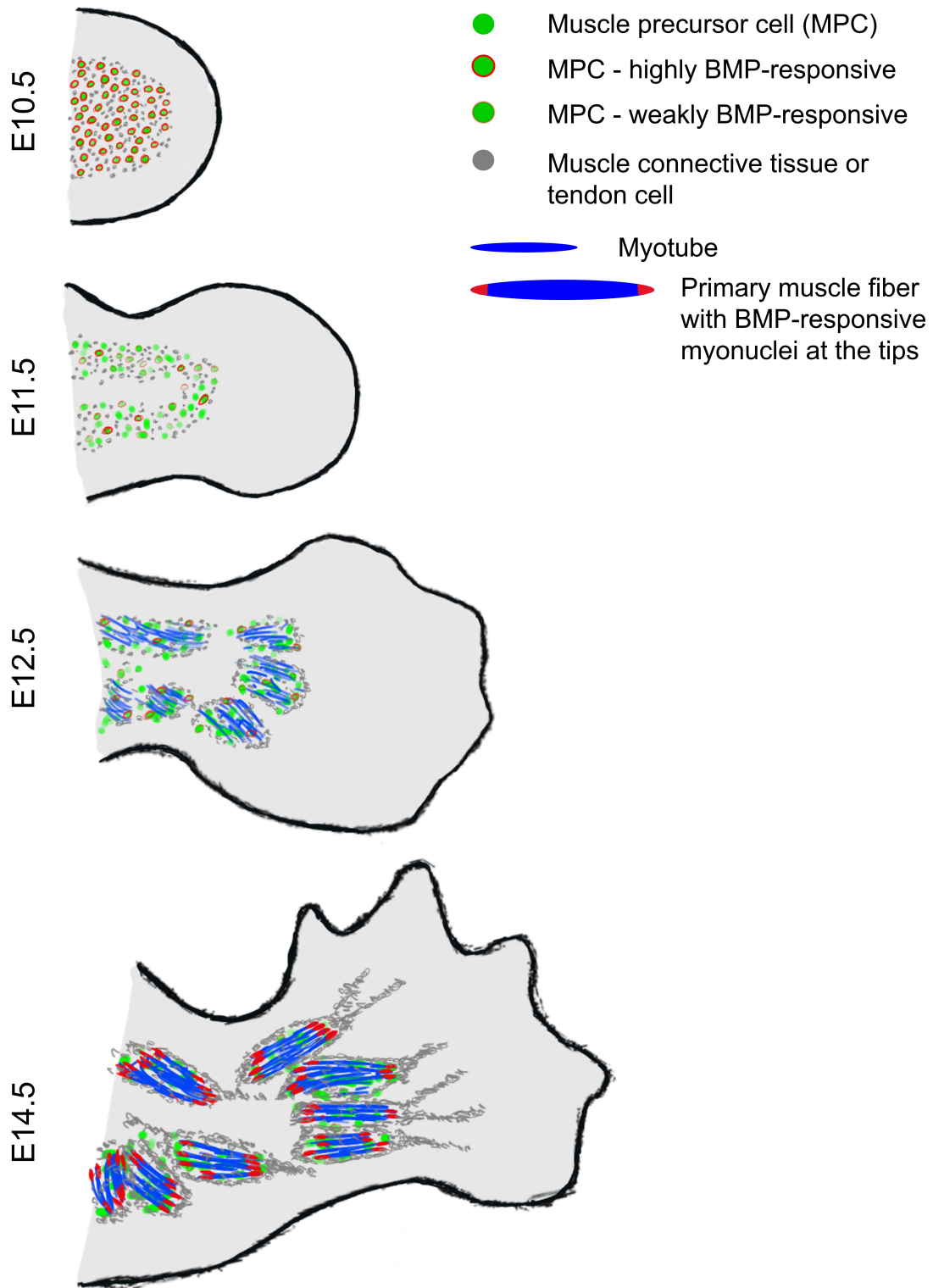


**Fig. S9. Schematic representation and model of forelimb buds, MPCs and muscle patterning between E10.5 and E14.5.**

**At E10.5:**

- All MPCs respond to BMP signaling.
- BMP signaling stimulates proliferation and distal migration, allowing MPCs to acquire future position along the proximo-distal axis.
- MPCs, while migrating, intermingle with future muscle connective tissue cells (e.g. TCF4<sup>+</sup> cells).

**At E11.5:**

- MPCs localise in clusters by following the prepattern established by muscle connective tissue cells.
- MPCs become less BMP-responsive as compared to E10.5.

**At E12.5:**

- The process of pre-muscle mass splitting continues, and individual muscle blocks become visible at E12.5, when first myotubes and primary myofibers form.

**At E14.5:**

- Muscle pattern is completely established.
- MPCs and primary muscle fibers are intermingled with muscle connective tissue cells.
- Muscle connective tissue increases around individual muscles (future perimysium) and elongates towards tendons.
- Primary fibers become BMP-responsive at their tips (at positions facing tendons).

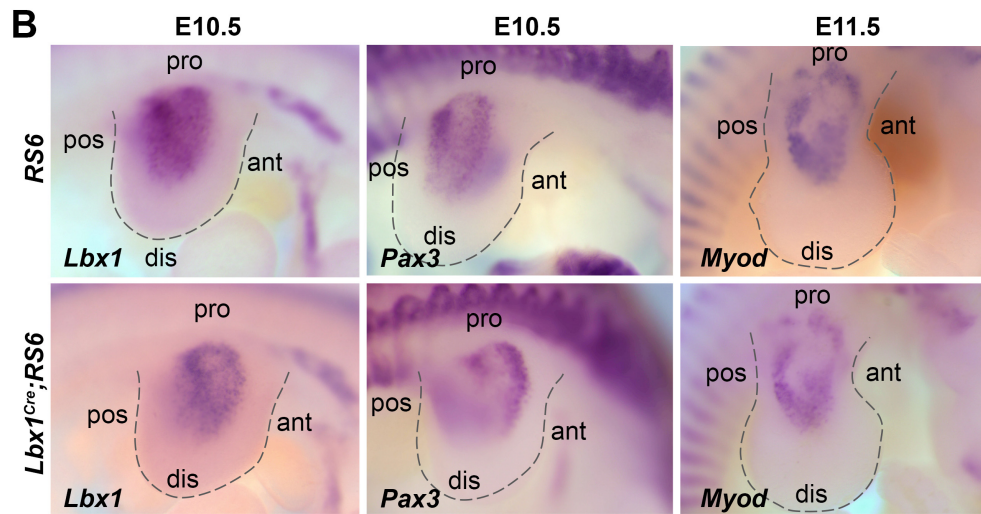
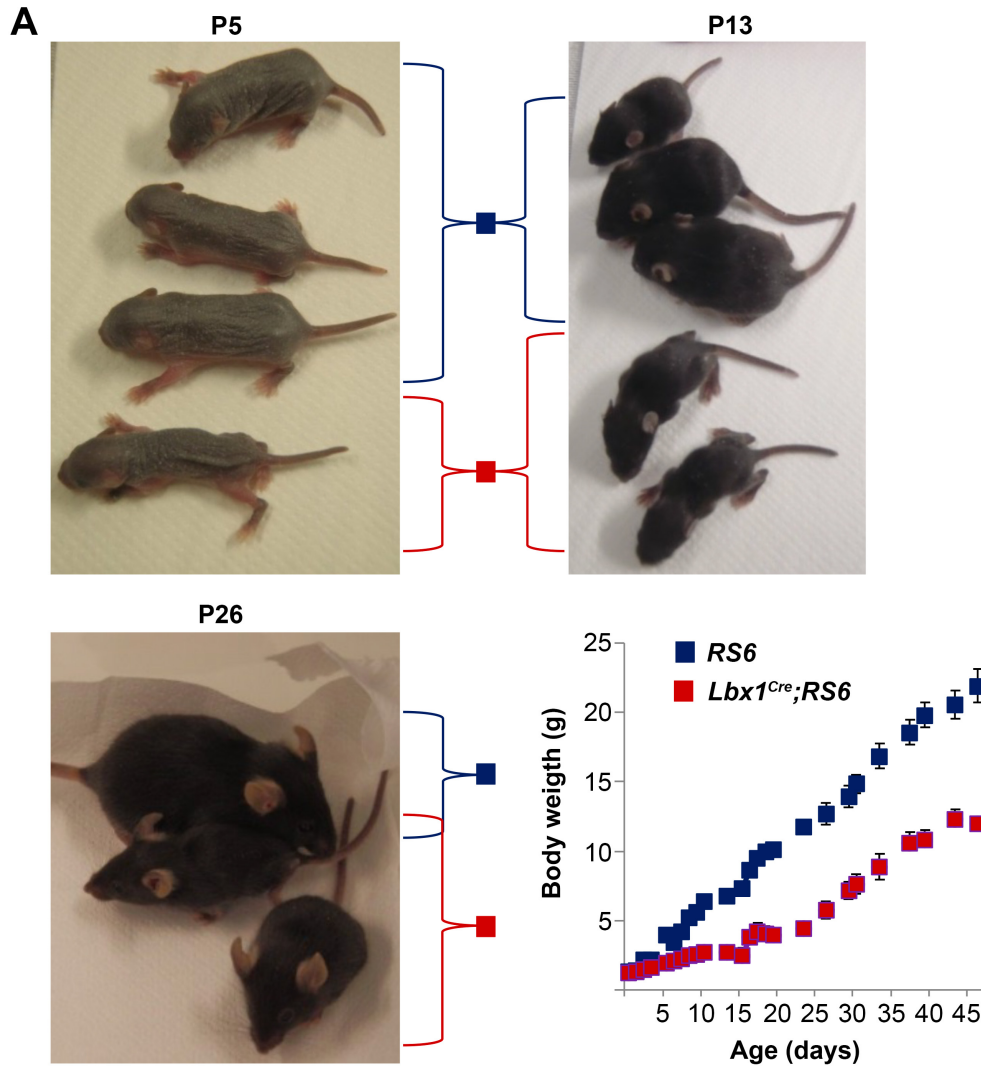




**Fig. S10. (A) Effect of *huSMAD6* overexpression on growth of postnatally surviving mice.** Images show of 5 day old (P5), 13 days old (P13), and 26 days old (P26) *RS6* and *Lbx1<sup>Cre</sup>;RS6* mice. The diagram blots the weight gain over the first 45 postnatal days of *Lbx1<sup>Cre</sup>;RS6* mice compared to *RS6* controls. Data points are depicted as mean  $\pm$  SE.

**(B) Effect of the heterozygous *Lbx1<sup>Cre</sup>* allele on the transcription of the early markers of forelimb muscle development.** Images depict the expression patterns of *Lbx1*, *Pax3* and *Myod* transcripts (purple) following WISH of E10.5 and E11.5 heterozygous *Lbx1<sup>Cre</sup>* embryos compared to that of *RS6* controls. Images show the dorsal view of the forelimbs, which are outlined by a grey dotted line (pro: proximal; dis: distal; ant: anterior; pos: posterior).

**Table S1. List of primers used for genotyping.**

Mice	Primer sequence (5' → 3')	Direction	Amplicon size
<i>Lbx1<sup>Cre</sup></i> mice	CGCCTTCCTCTCGCACCGTC	Forward	mutant: 432 bp
	GGCAGCCCCGGACCGAC	Reverse	
<i>RS6</i> mice	AAAGTCGCTCTGAGTTGTTAT	Forward	mutant: 249 bp wt: 585 bp
	GGAGCGGGAGAAATGGATATG	Reverse	
	CATCAAGGAAACCCTGGACTACTG	Reverse	
<i>Ai9</i> mice	AAGGGAGCTGCAGTGGAGTA	wt-Forward	mutant: 196 bp wt: 297 bp
	CCGAAAATCTGTGGGAAGTC	wt-Reverse	
	GGCATTAAAGCAGCGTATCC	mut-Forward	
	CTGTTCCCTGTACGGCATGG	mut-Reverse	
<i>HSA-Cre</i> mice	CCTGGAAAATGCTTCTGTCCG	Forward	mutant: 400 bp
	CAGGGTGTATAAGCAATCCC	Reverse	

**Table S2. List of primary antibodies used for immunohistochemistry.**

Target	Host	Clonality	Supplier	Reference	Dilution
Cleaved Caspase-3	Rabbit	mAb	Cell Signaling Technology	96645	1/800
Collagen 12	Rabbit	pAb (IgG)	Manuel Koch (Köln, Germany)	KR32/33	1:500
DsRed	Rabbit	pAb (IgG)	TakaraBio	632496	1:500
Laminin alpha-2	Rabbit	pAb (IgG)	Dako	Z0097	1:200
Laminin alpha-2	Rabbit	pAb (IgG)	Sigma-Aldrich	L9393	1:200
MHC	Mouse	mAb (IgG2a)	DSHB	A4.1025	1:20
MyoD	Rat	mAb (IgG2a)	Active Motif	39991	1:500
Myogenin	Mouse	mAb (IgG1)	DSHB	F5D	1:500
Pax3	Mouse	mAb (IgG2a)	DSHB	Pax3	1:100
Pax7	Mouse	mAb (IgG1)	DSHB	PAX7	1:10
pSmad1/5/9	Rabbit	mAb (IgG)	Cell Signaling Technology	13820	1:500
Tcf4	Mouse	mAb (IgG2a)	Merck	05-511	1:500
Hoxa11	Mouse	mAb (IgG3κ)	NovusBiologicals	5A3	1:200
Ki67	Rabbit	pAb (IgG)	Abcam	ab15580	1:500

**Table S3. List of secondary antibodies used for immunohistochemistry.**

Antibody	Conjugate	Supplier	Reference	Dilution
Goat anti-rabbit IgG (H+L)	A488	Thermo Fisher Scientific	A-11008	1:400
	A555		A-21428	
	A647		A-21070	
Goat anti-rat IgG (H+L)	A555		A-21434	
	A647		A-21247	
Goat anti-mouse IgG1	A488		A-21121	
	A555		A-21127	
	A647		A-21126	
Goat anti-mouse IgG2a	A488		A-21131	
	A555		A-21136	
	A647		A-21241	
Goat anti-mouse IgG3 $\kappa$	A555		A-21155	